Astron Astrophys Rev (2017) 25:3
https://doi.org/10.1007/s00159-017-0103-8

REVIEW

Major achievements of the Rosetta mission in connection with the origin of the solar system

M. A. Barucci[1] · **M. Fulchignoni**[1]

Received: 3 July 2017 / Published online: 24 October 2017

Abstract Comets have been studied from a long time and are believed to preserve pristine materials, so they are fundamental to understand the origin of the solar system and life. Starting in the early 1990s, ESA decided to have a more risky and fantastic mission to a comet. As Planetary Cornerstone mission of the ESA Horizon 2000 program, the Rosetta mission was selected with the aim of realizing two asteroid fly-bys, a rendezvous with a comet to deliver a surface science package and to hover around the comet from 4 AU inbound up to perihelion and outbound back to 3.7 AU. The mission was successfully launched on March 2, 2004 with Ariane V that started its 10-year journey toward comet 67P/Churyumov–Gerasimenko. After several planetary gravity assists, Rosetta flew by two asteroids—on September 5, 2008 (Steins) and on July 10, 2010 (Lutetia), respectively, and performed the comet orbit insertion maneuver on August 6, 2014. The onboard instruments characterized the nucleus orbiting the comet at altitudes down to few kilometers. On November 12, 2014, the lander Philae was delivered realizing the first landing ever on a comet surface. Although the exploration of the comet was planned up to the end of 2015, the mission duration was extended for nine more months than the nominal one, to follow the comet on its outbound orbit. To terminate the mission, following a series of very low orbits, a controlled impact of Rosetta spacecraft with the comet was realized on September 30, 2016. The scientific objectives of the mission have been largely achieved. The challenging mission provided the science community with an enormous quantity of data of extraordinary scientific value. In this paper, a detailed description of the mission and the highlights of the obtained scientific results on the exploration of an extraordinary

✉ M. A. Barucci
Antonella.Barucci@obspm.fr

[1] LESIA-Observatoire de Paris, CNRS, PSL, Université Pierre et Marie Curie, Université Paris Diderot, 92195 Meudon Principal Cedex, France

world are presented. The paper also includes lessons learned and directions for the future.

Keywords Rosetta space mission · Asteroid 2867 Steins · Asteroid 21 Lutetia · Comet 67P/Churyumov–Gerasimenko

1 Introduction

1.1 The science objectives for the Rosetta mission definition

When the Rosetta rider study (Bar-Nun et al. 1993; known as the "red book") was submitted to the approval of the ESA advisory committees, SSWG (today SSEWG) and SSAC, only three spacecraft encounters of small bodies' population had been done. The first took place on September 11, 1985, when the International Cometary Explorer (ICE) spacecraft passed through the tail of comet Giacobini–Zinner at a distance of 7800 km from the nucleus, providing in-situ information concerning the interaction of a cometary atmosphere with the solar wind plasma (Cawley 1987). The second took place in 1986, when comet Halley was approached and observed by an "international armada" (Newburn 1986) of five space probes [Giotto (ESA), which flew by the nucleus as close as 596 km, Vega 1 and Vega 2 (USSR/France Intercosmos), Suisei, and Sakigake (ISAS)]. The third one realized the first fly-by of an asteroid in 1991 when the NASA Galileo probe in its journey toward Jupiter flew by the main belt asteroid Gaspra (Veverka et al. 1994). These missions provided the ground truth in interpreting the largest wealth of information on small bodies' population obtained from ground and in orbit observations: it became evident that the small solar system bodies, asteroids and comets, play a key role in understanding the primordial phases of the solar system formation: they constitute an almost continuous suite of progressively less evolved objects, which preserve quite intact the pristine material from which the swarms of planetesimals formed about 4.6 billions years ago. Since then in fact, comets have been submitted to very low levels of evolutionary pressure, and the differentiation of some larger asteroids has been spread over at most the first few million years: so, small bodies contain materials which witnessed the early phases of the formation of the solar system.

Already in 1991, the European Space Agency (ESA) chose as Planetary Cornerstone mission of its Horizon 2000 program the Rosetta mission, a rendezvous with a comet and one or two fly-bys of asteroids, realized by an orbiter spacecraft delivering a surface science package to the surface of the comet. The Rosetta Science Team which prepared the rider study outlined three viewpoints under which the scientific objectives of the mission had to be considered:

- The close relationship of small solar system bodies with early planetesimals. Particularly, the study of their material in situ, as more primitive than any other available extraterrestrial material, e.g. meteorites which were processed by solar radiation and atmospheric entry.
- The study of the physical–chemical processes that are specific to comets and asteroids. Asteroids can shed light on impact phenomena and collisional evolution of

the small bodies population, cometary activity represents one of the most complex process to be observed in the solar system. Chemistry, physics, geochemistry and geophysics are necessarily involved in these studies.
- The necessity to increase the level of in-depth knowledge of small bodies, which in terms of diversity constitute an inexhaustible reservoir of information concerning the origin and the evolution of the solar system.

The Rosetta mission has been specifically designed to achieve these scientific goals, focusing on remote sensing investigation for both the asteroids, the comet and on in situ investigations of cometary materials. A lander, later named Philae, was designed to provide information on the chemical and physical properties of a selected area. Dust grains and gas flowing out from the nucleus, captured from the orbit, were planned to be analyzed by sophisticated instruments onboard the orbiter, to define their nature and to link the materials in the coma to volatile and refractory species in the nucleus.

1.2 Rosetta's journey and the mission targets

The original targets of the Rosetta mission were comet 46P/Wirtanen and the asteroids (140) Siwa and (4979) Otawara. The launch, scheduled for January 2003, was postponed to the beginning of March 2004, because of a problem due to the thermal shield of Ariane V launcher during the countdown. This delay obliged the Rosetta navigation and Science Teams to define a new mission baseline. They selected the comet 67P/Churyumov–Gerasimenko as the main target, while the asteroids (21) Lutetia and (2867) Steins were chosen (Barucci et al. 2005) after the spacecraft interplanetary orbit insertion maneuver, when the available amount of ΔV was known.

The mission was successfully launched on March 2, 2004 with Ariane V from Kouru, French Guynea. The spacecraft started its journey (Fig. 1) to the comet 67P/Churyumov–Gerasimenko, after three Earth and one Mars gravity assist and the fly-bys of the two asteroids that took place on September 5, 2008 (Steins) and on July 10, 2010 (Lutetia). Then, in June 2011, the probe was put in a state of deep space hibernation during 31 months, with all the onboard systems maintained at the lower vital level, to reduce the consumption of energy during the phase of the its trajectory most far away from the sun.

After the "wake-up" and a complete check of all the onboard systems, the navigation system started the maneuvers aimed at the rendezvous with the comet. The first images where the comet 67P/Churyumov–Gerasimenko started to be resolved were obtained in July 2014, revealing that the shape of the comet is a complex double-lobed structure with a 'head' and a 'body' separated by a neck (Fig. 2). On August 6, 2014, Rosetta encountered the comet after more than 10 years of interplanetary cruise and joined it in its journey around the Sun.

The first 6 weeks of activity of the Rosetta probe were dedicated to the global coverage of its surface to get its physical bulk properties (mass, shape, density, topography, morphology, etc.) and to characterize the effects of the activity on its immediate environment (gas, dust, interaction with the solar wind, etc.) to select a landing site for Philae. The OSIRIS camera was used to map the entire surface at the highest resolution to select the best landing site for Philae. Detailed maps showing all the dan-

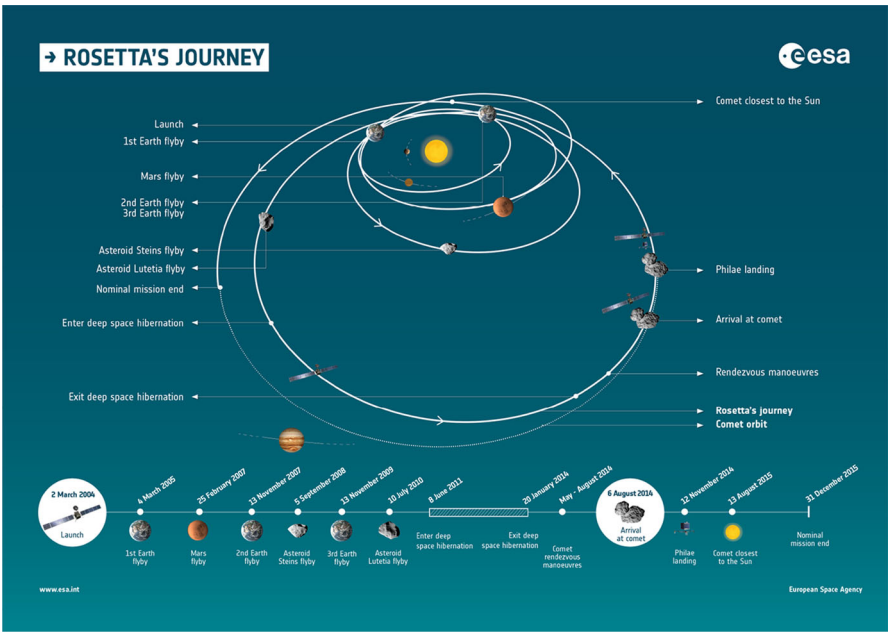

Fig. 1 Rosetta probe trajectory toward the 67P/Churyumov–Gerasimenko and the main phases of the mission (ESA courtesy)

Fig. 2 First view of the comet 67P/Churyumov–Gerasimenko shape as imaged on July 14, 2014 by OSIRIS imaging system, from a distance of approximately 12,000 km (ESA/Rosetta/MPS for OSIRIS Team MPS/UPD/LAM/IAA/SSO/INTA/UPM/DASP/IDA)

gerous slopes, crevasses and boulders were prepared. Between the end of August and October 2014, a preliminary selection of several possible candidate sites was made, using the observations in assessing their respective scientific merits, while the Rosetta Mission Operations Centre carried out a comprehensive analysis to identify possible trajectories to deliver the lander, and to confirm that the proposed landing sites could be reached with the required accuracy. Finally, a site (J in Fig. 3), later called Agilkia region situated on the smaller lobe, was selected as the primary landing site, and another area (C in Fig. 3), on the larger lobe, as the backup site. On November 12, the landing took place entirely automatically on the primary landing site.

The exploration of the comet continued during and after its approach to the perihelion (August 13th, 2015). An extended post-perihelion mission for a period of 9 months (initially the end of the mission was scheduled for December 31, 2015), was

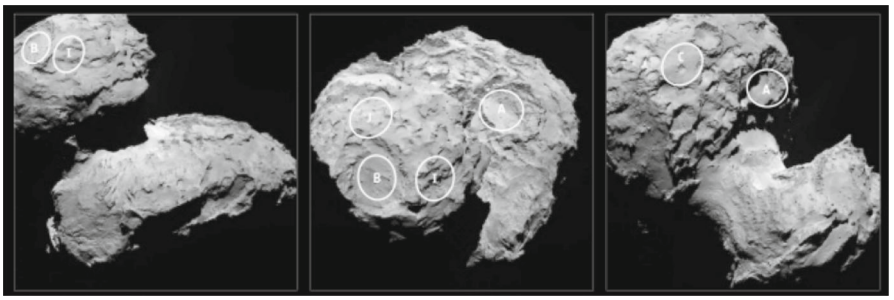

Fig. 3 Five of the candidate sites identified on comet 67P in August 2014. The approximate locations of the five regions are marked on these OSIRIS narrow-angle camera images taken on August 16 from a distance of about 100 km (ESA/Rosetta/MPS for OSIRIS Team MPS/UPD/LAM/IAA/SSO/INTA/UPM/DASP/IDA)

decided to move the orbiter much closer to the comet's nucleus as the cometary activity diminished. The objective was to make a detailed survey of changes in the comet's properties during its brief 'summer'. As the comet was far away from the Sun again, there was no longer enough solar power to run Rosetta's set of scientific instrumentations efficiently: on September 30, 2016, the final act of the Rosetta mission was the controlled descent of the probe to the comet surface.

The obtained main bulk properties of the two flown-by asteroids and the comet nucleus are reported in Table 1.

1.3 The philosophy in selecting the payload

The Rosetta orbiter analyzed comet 67P/Churyumov–Gerasimenko and its environment using a suite of 11 instruments to meet the scientific objectives described above. In particular, three instruments were specifically conceived for determining and characterizing the global properties of the cometary nucleus and the asteroids flown by during the cruise phase :

- the optical, spectroscopic, and infrared remote imaging system (OSIRIS), a dual camera imaging system consisting of a narrow angle (NAC) and wide angle camera (WAC) operating in the visible, near infrared and near ultraviolet wavelength range (Keller et al. 2007);
- the radio science investigation (RSI) to measure the nucleus mass and to infer details of the comet environment tracking the motion of the spacecraft (Pätzold et al. 2007);
- the comet nucleus sounding experiment by radio wave transmission (CONSERT) studying the internal structure of the comet interacting with a transmitter/receiver mounted on the lander Philae (Kofman et al. 2007).

The composition of the asteroid and nucleus surfaces as well as that of the coma has been investigated by three spectrometers covering a wide spectral range from UV to microwaves and by a sophisticated mass spectrometer:

- the ultraviolet imaging spectrometer (Alice), characterizing the composition of the comet nucleus and coma (Stern et al. 2007);

Table 1 Summary of the bulk properties of the two asteroids and the comet 67P

Asteroids	Dimensions (km)	Rotation (h)	Spin axis (α, δ)	Albedo	Mass (kg)	Density kg m^{-3}	Temperature (K)	D/H
(2867) Steins	$6.8 \times 5.7 \times 4.4$	6.047	99° +59°	0.41	–	–	185–225	–
(21) Lutetia	$121 \times 112 \times 87$	8.168	51.8° +10.8°	0.19	$1.7 \times 10^{18} \pm 0.01$	3400 ± 210	170–245	–
67P/Churyumov–Gerasimenko	body: $4.1 \times 3.5 \times 1.6$	12.404	69.3°	0.06	$9.982 \times 10^{9} \pm 0.003$	532 ± 7	180–230	$5.3 \pm 0.7 \times 10^{-4}$
	head: $2.5 \times 2.1 \times 1.6$		+64.1°					

- the visible and infrared thermal imaging spectrometer (VIRTIS), studying the nature of the asteroids, the comet nucleus and the gases in the coma (Coradini et al. 2007);
- the microwave instrument for the Rosetta Orbiter (MIRO), investigating the nature of the cometary nucleus, outgassing from the nucleus and development of the coma (Gulkis et al. 2007);
- Rosetta orbiter spectrometer for ion and neutral analysis (ROSINA) determining the composition of the comet's atmosphere and ionosphere, and measuring the temperature, velocity and density of the gas flow, comprising: a double-focusing mass spectrometer (DFMS), a reflection time-of-flight mass spectrometer (RTOF) and a comet pressure sensor (COPS) (Balsiger et al. 2007).

Three instruments were dedicated to the study of cometary dust that were complemented by specific measurements carried out by OSIRIS, Alice, VIRTIS:

- grain impact analyzer and dust accumulator (GIADA) measuring the number, mass, momentum and velocity distribution of dust grains in the near-comet environment (Colangeli et al. 2007);
- cometary secondary ion mass analyzer (COSIMA) studying the dust structure and composition in the comet's coma (Kissel et al. 2007);
- micro-imaging dust analysis system (MIDAS) studying the dust environment of the comet (Riedler et al. 2007).

The plasma environment of the comet has been investigated by the Rosetta plasma consortium:

- RPC: a six-component experiment comprising an ion composition analyzer (ICA, Nilsson et al. 2007), an ion and electron sensor (IES, Burch et al. 2007), a Langmuir probe (LAP, Eriksson et al. 2007), a fluxgate magnetometer (MAG, Glassmeier et al. 2007), a mutual impedance probe (MIP, Trotignon et al. 2007) and a plasma interface unit (PIU, Carr et al. 2007).

Moreover, the "in situ" measurements obtained by the instruments onboard the lander Philae provided some key information on the nature of the comet, as described in more detail in Sect. 4.

1.4 The navigation toward and around the comet

The navigation team of Rosetta can be highly praised for the great success of the mission. They were maneuvering the spacecraft during more than 10 years in its cruise toward the comet and found an incredible succession of orbits and fly-bys around/over the comet that allowed the onboard instrumentation to meet all the mission scientific objectives and much more.

After the launch, Rosetta utilized four planetary swing-by maneuvers (gravity assists) to get the correct velocity to reach the comet. The first swing-by was around Earth and took place 1 year after the launch on March 4, 2005 (Morley and Budnik 2006). The second swing-by, around Mars, took place on February 25, 2007 (Budnik and Morley 2007), and in terms of navigation the Mars swing-by has been the most

demanding because it was a swing-by around a distant planet at 2.1 AU and the nominal pericenter altitude was only 250 km above the surface of Mars. It was followed soon after by a second Earth swing-by on November 13, 2007, and by the fly-by of the asteroid (2867) Steins (Morley and Budnik 2009). Rosetta returned to Earth in November 2009 to get its final boost to fly by the asteroid (21) Lutetia (Morley et al. 2012) and proceed toward the comet. From June 8, 2011, the spacecraft was put into deep-space hibernation, with virtually all systems shut down. This operation was necessary because of Rosetta's increasing distance from the Sun did not allow the solar panels to produce enough power. After 31 months, on January 20, 2014, the spacecraft was woken up and started the final approach to the comet with a complex suite of approaching orbits (see the site: http://blogs.esa.int/rosetta/2016/12/23/rosettas-complete-journey-animation).

The spacecraft arrived at a distance of 100 km from the nucleus of the comet on August 6, 2014, then gradually approached the comet along specific mapping orbits to select a landing site for Philae. The maneuvers to perform Philae's release took place on November 12, 2014. Then, Rosetta settled into longer-term science orbits, including several more or less closer fly-bys. Approaching the perihelion (August 2015), on account of the comet's increased activity, for its safety Rosetta remained well beyond 100 km for several months. Following the closest approach to the Sun, Rosetta made a dayside far excursion some 1500 km from the comet, while in spring 2016 Rosetta went on a nightside excursion, followed by a very close fly-by and orbits dedicated to science observations.

When the orbit of the comet started to be far from the Sun again and the amount of sunlight reaching Rosetta's solar panels decreased, combined with an aging spacecraft and payload that have endured the harsh environment of space for over 12 years, the ESA engineering team decided to guide Rosetta down to the comet surface with a controlled impact. Thus in early August 2016, the spacecraft started its progressive descent toward the comet. On September 24, Rosetta started a 16×23 km orbit used to prepare the final descent. On the evening of September 29, Rosetta began the final slow descent onto the nucleus from an altitude of 19 km, gently striking the surface at 10:39 GMT on September 30, concluding the mission.

2 Science during the planet fly-bys

On March 4 and 5, 2005, the ROSETTA probe performed the first of its three fly-bys of the Earth; at its closest approach, the probe passed at less than 2000 km from ground. The MIRO instrument has been able to measure various instrument performance parameters using the Earth, Moon, Venus and two comets as sources of input signals (Gulkis et al. 2007). To verify the VIRTIS performances conditions, several images of the Earth were acquired during the outbound trajectory after the closest approach when the Earth was already at a distance of 248000 km. The typical spectra of the dayside and of the nightside were compared to the average spectrum of the Earth observed by NIMS onboard Galileo. All the most important atmospheric molecules, H_2O, CO_2, CH_4, O_3, N_2O, were visible in all the VIRTIS spectra (Coradini et al. 2010). The five instruments of the Rosetta Plasma Consortium (RPC) were

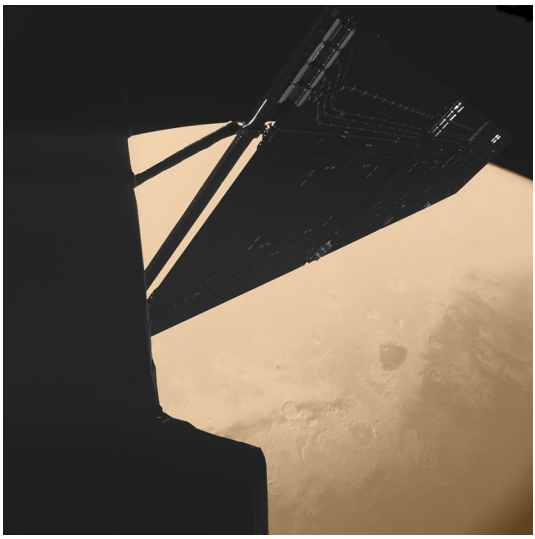

Fig. 4 CIVA camera onboard the Rosetta's Philae lander took this image 4 min before the closest approach of Mars, at a distance of 1000 km (ESA courtesy)

switched on in the plasmasphere, the high electron-density region dominated by the Earth's magnetic field, for calibration and testing purposes. The mutual impedance probe (MIP) determined the electron plasma density and temperature (Trotignon et al. 2005) as well as the magnetic field strength (Trotignon et al. 2006).

On February 25, 2007, Rosetta passed just 250 km from the surface of Mars. The CIVA camera, on Philae lander, imaged one of Rosetta's 14 m-long solar panels, set against the northern hemisphere of Mars, and the details in the Mawrth Vallis region can be seen in Fig. 4. The lander magnetometer ROMAP was switched on too: the collected data provided insights into the plasma environment around Mars: (1) a pronounced bow shock crossing, (2) the signatures of the pile-up region of draped magnetic field and (3) the signatures of crustal magnetic field anomalies (Boesswetter et al. 2009). During the gravitational assist maneuver, the Rosetta OSIRIS NAC camera took several images of the Mars atmosphere and surface partially covered by clouds which were carefully analyzed by Pajola et al. (2012a, b). Moreover, the geometry of this fly-by gave the chance to obtain a number of Rosetta OSIRIS images of Phobos before and after Rosetta–Mars closest approach. The comparison of the spectra (obtained through the NAC filters) during the pre- and the post-closest approach, with the reflectance spectra of D-type asteroids, shows that Phobos near-ultraviolet, visible and near-infrared reflectivity is within the spectral dispersion of the D-type asteroids. The possibility of a dynamical collisional capture of Phobos similar to the origin of the irregular satellites of the giant planets has been studied: the observational and dynamical coupled results suggest an early capture of Phobos in the first 10–100 My of the lifetime of the solar system (Pajola et al. 2014). The Alice instrument was used to study the daytime Mars upper atmosphere including emissions from exospheric hydrogen and oxygen: these data allowed the Alice team to detect and map the H Lyman-α and Lyman-β emissions from exospheric hydrogen, out beyond 30,000 km from the planet's center (Feldman et al. 2011).

The OSIRIS camera and the navigation camera (NAVCAM) onboard Rosetta observed again the Earth during its second and third swing-bys in November 2007 and November 2009, respectively.

3 The asteroid encounter

The final choice of the asteroid fly-by targets was made only after the successful launch of the spacecraft and the first orbital correction maneuver to evaluate the available ΔV to be used to fly by the asteroids. After analyzing all the possible candidates proposed by the Rosetta Project before the launch, Barucci et al. (2005) recommended the selection of (21) Lutetia and (2867) Steins for their high potential scientific return. Lutetia was selected mostly because of its large size, which allowed the RSI to mesure an accurate mass and determine the density. Steins was selected for its unusual surface composition, similar to the rare E-type class, which had never been observed by space missions before.

On September 5, 2008, the fly-by with Steins took place at a relative velocity of 8.6 km s^{-1} with a closest approach distance of 803 km. On July 10, 2010, the fly-by of Lutetia was performed at a velocity of 15.0 km s^{-1} with a closest distance of 3168.2 km. Four instruments performed imaging and spectrometric observations from the ultraviolet (70 nm) through the visible and infrared to the millimeter range (1.3 mm).

3.1 Steins, a diamond in the sky

(2867) Steins was observed by the OSIRIS imaging system, with the narrow-angle camera (NAC) and the wide-angle camera (WAC) acquiring resolved images starting 4 h before the closest approach at a distance of about 60,000 km. The obtained images covering 60% of the surface showed a diamond-shaped object (Fig. 5) with dimensions of $6.8 \times 5.7 \times 4.4$ km^3 and a best resolution of about 80m/pixel (Keller et al. 2010). The asteroid has a rotational period of 6.04679 ± 0.00002 h with the pole almost perpendicular to the ecliptic plane and a geometric albedo of 0.41 ± 0.016.

Steins exhibits a surface covered by shallow craters, pits, ejecta and regolith (Fig. 5). Near the south pole, there is a large crater of 2.1 km in diameter (named Diamond) and a series of circular features (catena) of 250–600m in diameter extending from this crater to the north side. This catena may be linked to the impact that caused the larger crater. Based on analysis of the images, Steins can be considered a rubble-pile body. About 42 crater-like depressions were identified on the surface and the crater population seems to exhibit a dichotomy between the two sides of Steins (Besse et al. 2012). The poor presence of small craters can be interpreted by a number of processes responsible for small crater erasing, as seismic shaking produced by small impacts or by the formation of the Diamond impact crater.

To investigate Steins' age, Marchi et al. (2015) studied the cumulative crater size–frequency distribution (SFD), finding it to be remarkably shallow and comparable to that of Itokawa and Eros for crater sizes smaller than 0.1 km. An interpretation for this shallow slope is the possible erosion of small craters. An alternative possibility is that many of the observed crater-like features are not impact craters, but rather

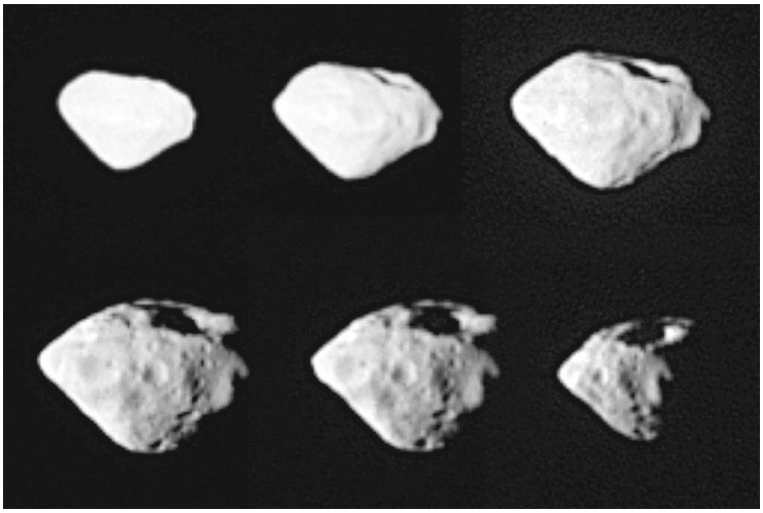

Fig. 5 Steins images taken on September 5, 2008. On the top, NAC images with best resolution (top right: 100 m/px) at a distance of 5200 km and phase angle of 30°. On the bottom, WAC images with the left one at the best resolution (80 m/px) taken at a distance of 806 km. The south pole is up with the large Diamond crater clearly evident, approximately 1.5 km in size. (ESA/Rosetta/MPS for OSIRIS Team MPS/UPD/LAM/IAA/SSO/INTA/UPM/DASP/IDA)

drainage pits caused by regolith sinking into sub-surface fractures and voids. Jutzi et al. (2010) simulated the impact resulting in the Diamond crater and concluded that the impact would have damaged a monolithic parent body, and transformed Steins into a rubble pile structure and reshaping it by the YORP (Yarkovsky–O'Keefe–Radzievskii–Paddack) spin-up thermal effect. The interpretation of Steins' shape as being the result of YORP evolution implies that mass wasting of loose regolith may also have contributed to the erasure of the majority of the craters. In fact, Steins shows an equatorial ridge (Keller et al. 2010), which can be formed by centrifugal acceleration as the asteroid was spun up by the YORP effect with the migration of the regolith from the polar regions toward the equator, thereby forming the ridge. The determination of the absolute cratering retention age of Steins is therefore challenging and the age estimate highly uncertain. Fitting the largest craters (>0.6 km), the surface age is estimated at ∼1.3 Ga, but it should be considered only as an upper uncertain limit.

The imaging-spectrometer VIRTIS-M, observing Steins from 200 to 5000 nm and the OSIRIS camera system observing the asteroid with 11 filters from 220 to 960 nm, confirmed the surface composition similar to typical rare E-type asteroid. The spectra show a reddening at wavelengths < 1000 nm with a strong signature at 490 nm, a steep drop below 400 nm, and almost flat and featureless for wavelengths > 1000 nm. The characteristic absorption feature at 490 nm is attributed to sulfides. The spectra are similar to those for which the main mineralogical components are enstatite and oldhamite with small amounts of low-iron silicate mineral. The surface temperature of Steins was also measured giving a minimum and maximum value of 185 and 225 K with a mean thermal inertia of 110 J m^{-2} $K^{-1}s^{-1/2}$, which implies a thick layer of regolith (Leyrat et al. 2010).

3.2 Lutetia, a differentiated small world

The OSIRIS camera systems observed the asteroid (21) Lutetia for about 10 h around the closest approach, with different filters covering more than 50% of the surface with spatial resolutions larger than 60 m/pixel (Sierks et al. 2011). The global shape has the principal axes dimensions of $121 \pm 1 \times 101 \pm 1 \times 75 \pm 13$ km^3 with north pole ecliptical coordinates of $51.8° \pm 0.4°$ and + $10.8° \pm 0.4°$ (Sierks et al. 2011) and a rotational period of 8.168271 ± 0.000002 h. The volume estimation is uncertain following the fact that a large fraction of the asteroid's southern hemisphere was not visible during the fly-by and consequently the shortest semi-major dimension is not well constrained. A bulk density of 3400 ± 300 kg m^{-3} was computed combining the estimated volume and the mass obtained by the Radio Science Investigation (RSI) (1.7×10^{18} kg $\pm$ 1%) (Pätzold et al. 2011). The visible albedo is 0.19 ± 0.02 with surface variations in reflectivity up to 30% correlated with geographic morphologies (Sierks et al. 2011).

The north rotational pole was pointed toward the Sun at the time of the Rosetta encounter and hence high-resolution imaging was restricted by the illumination to one hemisphere. Some parts of the northern hemisphere were not well imaged because of the low phase angle of the approach ($\sim 7.7°$). The north pole is located near a depression that has been produced by multiple impacts—the North Polar Crater Cluster (NPCC) (Fig. 6).

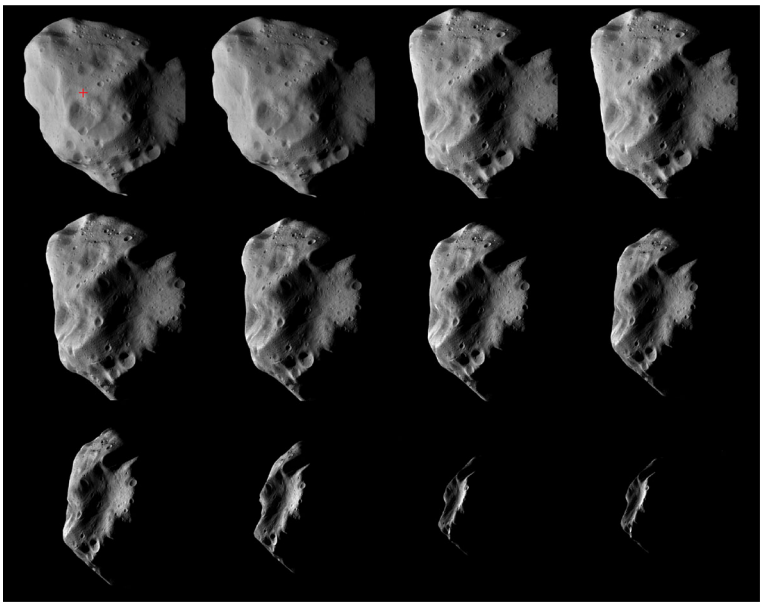

Fig. 6 (21) Lutetia NAC images taken on July 10, 2010 during the fly-by. Upper left at a distance of 3604 km, upper right is the close encounter and mid from 3207 to 3667 km. Low: 3915, 4628, 6072, 6304 km. The red cross on the top left image indicates the north pole close to the NPCC. The large depression Massilia on the right of the image is clearly evident (ESA/Rosetta/MPS for OSIRIS Team MPS/UPD/LAM/IAA/SSO/INTA/UPM/DASP/IDA)

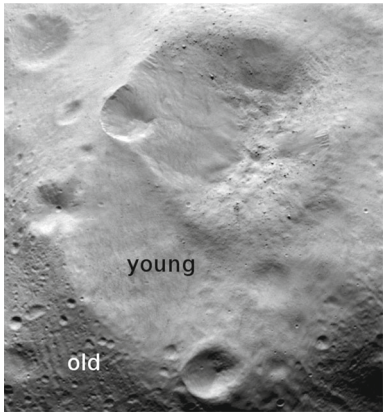

Fig. 7 The central portion of the image taken by NAC showing the NPCC. The Gades impact crater is toward the top. Boulders are also evident on the top of the image in the NPCC. The largest visible boulder is about 250 m in width (ESA/Rosetta/MPS for OSIRIS Team MPS/UPD/LAM/IAA/SSO/INTA/UPM/DASP/IDA)

All of the surface is dominated by impact craters. The largest depression is the Massilia crater-like structure (see Fig. 6), with a diameter of 57 km and a rim which appears to have been modified by subsequent impacts. The area in the NPCC is one of the youngest surfaces on the object with relatively low density of smaller impact craters (see Fig. 7). Lutetia possesses also a remarkable set of lineaments, some of which are > 80 km long. Among several interpretations, Besse et al. (2014) suggested that impacts produce circumferential lineaments and which could require production via three separate impacts, one of which is on the unobserved hemisphere. Inside and around the NPCC, there is a large number of boulders (Küers et al. 2012) which are up to 250 m in size. The low surface gravity may have played a role in producing a more complex spatial distribution of boulders with respect to the impact. Assuming that boulders are broken down with time by micro-meteorite impacts together with assumptions about the impact rates, Küers et al. (2012) constrained the surface age of the NPCC to $\sim$300 million years. The interior of NPCC of Lutetia shows evidence of landslides, with one seeming to be a debris slide or avalanche about 10 km wide and having several lobes of 200 m scale relief at its base (see Fig. 7). The landslides seem to have resulted in the most recently produced surfaces on Lutetia.

The surface of Lutetia has been divided by different geological regions (Thomas et al. 2012). It shows abundant impact craters, whose spatial distribution appears highly variable across the surface even if the illumination conditions due to the geometry of the fly-by did not allow an uniform detection of craters across the imaged surface for the variable spatial resolution. The Achaia region exhibits the highest crater density. The overall distribution of craters revealed 157 craters larger than $\sim$ 0.6 km. The Narbonensis region corresponds to the floor of the largest impact structure on Lutetia, Massilia crater. Baetica is the youngest region and shows very few small impact craters. The region appears to have been produced by the formation of three superposed large impact structures with a subsequent smaller impact.

The absolute surface age determination requires some assumptions on the crater scaling law and mechanical properties of the target (Marchi et al. 2012, 2015) with an age varing from $\sim$ 2.6 to 3.3 Ga. The region with a thick layer of regolith can be around 100 million years old.

The surface, as observed by VIRTIS-M hyperspectral images, shows flat and featureless visible and near-infrared spectra and did not allow discriminating between a carbonaceous and/or enstatite nature. The 3000 nm band was not observable by VIRTIS instrument on the visible 50% of the Lutetia's surface (Coradini et al. 2011), although the other surface of the asteroid, not visible to Rosetta, showed the hydration feature (Rivkin et al. 2011). Barucci et al. (2012), assembling all the available data from UV to mid-infrared and polarimetric data, argued that the analogies with existing meteorites remain inconclusive. The complex composition can be explained with local variations connected to different compositions and different surface textures and regolith. The surface is probably composed of different chondritic-like materials. Regions in the southern hemisphere seem to be dominated by carbonaceous chondrites with the presence of aqueous altered materials, while regions in the northern hemisphere could be connected to a mixture of enstatite and carbonaceous chondrites. The UV ALICE spectrometer observed Lutetia from 70 to 205 nm (Stern et al. 2011) and detected the strongest feature in the spectra with a drop between 180 and 160 nm.

Temperature variations between 170 and 245 K and correlations with topographic features were detected using VIRTIS observations with a thermal inertia of 20–30 J m^{-2} K^{-1} $s^{-1/2}$ (Coradini et al. 2011). This suggests a small-scale roughness with a surface layer of high porosity.

Thanks to the measure of mass and the estimation of volume, a higher than expected bulk density of 3400 ± 300 kg m^{-3} (Pätzold et al. 2011) has been computed, which leads to speculation that Lutetia (Weiss et al. 2012) could have experienced an early thermal metamorphism and could have a partially differentiated metallic core overlaid by a primitive chondrite crust.

3.3 Progress in understanding the nature of asteroids

The two asteroids visited by the Rosetta mission are complex worlds with properties completely different from asteroids previously visited by the spacecraft. The analyzed data gave important information on the history of the two asteroids. Lutetia and Steins are different in shape, size, albedo, composition, density, surface morphology and evolution. Though fly-bys give limits connected with the velocity of the encounter and the geometry of the trajectory, which rapidly changes the viewing geometry and limit the collected data, the obtained data provided precious information on the surface of the visited asteroids.

The small asteroid Steins seems to have undegone a combination of various processes, such as impacts, seismic shaking and YORP effect which are necessary to explain its present physical characteristics. The large-size asteroid Lutetia shows a high-density body with a complex geological surface exhibiting pits, craters, scarps and vast younger terrains. The surface seems to be primordial, with a possible differentiated metallic core. The surface material motion detected on Lutetia could be expected on other asteroids. On large asteroids like Lutetia, crater SFDs allow detailed studies with relative ages of various units and absolute ages. The imaging resolution is good enough to obtain robust crater statistics.

Spectral observations give good information on the possible composition, though the lack of clear, recognizable absorption bands might not allow interpretation of the

real composition of the surface. In fact, all the detailed analyses of the data obtained during the fly-bys do not allow us to unveil the real composition of Steins and Lutetia, for which only a sample return mission will reveal the composition of these intriguing objects.

The two asteroid fly-bys allowed to collect precious data of high scientific value and provided the scientific community with a ground truth for checking the methods to interpret the ground-based observations, able to characterize a larger number of asteroids. The future sample return space missions (OSIRIS-Rex by NASA and Hayabusa-2 by JAXA) will allow to analyze with sophisticated laboratory instruments the samples collected on the surface and to determine the real composition of the visited asteroids.

4 Philae

4.1 Philae's landing sequence

The box-shaped lander Philae was carried piggyback on the side of the Orbiter until its arrival at comet 67P. Once the orbiter was aligned correctly in a hyperbolic trajectory with a 5 km miss distance to the comet nucleus, almost on a collision course with the comet, the ground station commanded the lander to self-eject from the main spacecraft and unfold its three legs, ready for a gentle touchdown. The separation occurred at an altitude of about 20.5 km on November 12, 2014.

After almost 7 h of ballistic descent (Fig. 8), Philae landed at 15:34:03.98, in Agilkia region (formerly called "area J"; see Fig. 3) on 67P, as registered by the SESAME-CASSE accelerometer. Two subsystems of the lander, a cold gas system to push it to the surface and two anchoring harpoons to fix it to the ground, were planned to be activated at the touchdown. Unfortunately, both subsystems did not work, leading the lander to bounce several times before coming to rest after about 2 h of ballistic flights. OSIRIS NAC images were used together with ROLIS descent images for determining

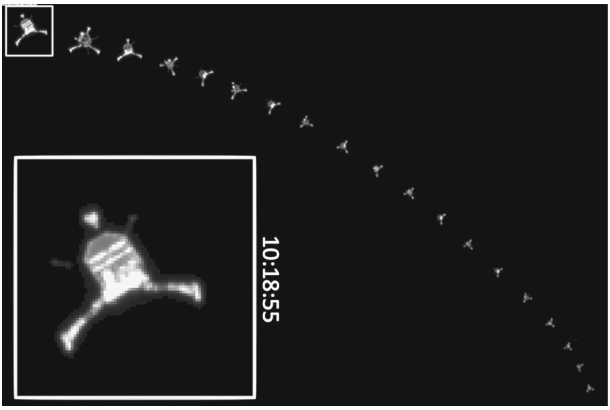

Fig. 8 Sequence of images of the Philaes' descent toward the comet taken by the OSIRIS camera after separation (ESA/Rosetta/MPS for OSIRIS Team MPS/UPD/LAM/IAA/SSO/INTA/UPM/DASP/IDA)

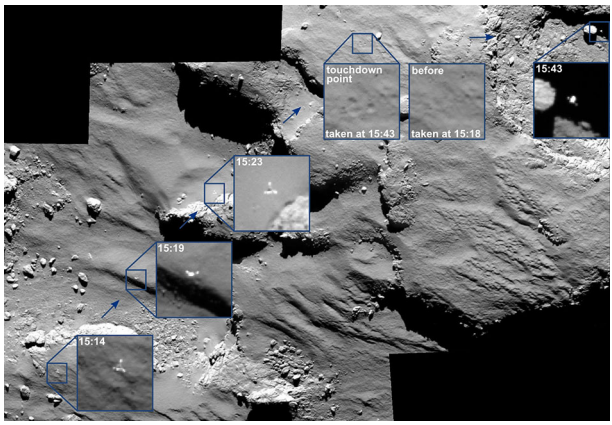

Fig. 9 Osiris image of the Agilkia region, the area of the first Philae touchdown (TD1). The superposed boxes show three positions of Philae before landing (at 15:14, 15:19 and 15:23, respectively), the initial landing site (before and after the touchdawn) and its first rebound (TD2 at 15:43) (ESA/Rosetta/MPS for OSIRIS Team MPS/UPD/LAM/IAA/SSO/INTA/UPM/DASP/IDA)

the actual landing coordinates and attitude at Philae's first landing site. The descent and bouncing trajectory of Philae has been reconstructed using observations of the lander in the OSIRIS wide-angle camera (WAC) and NAVCAM images, the CONSERT measurements and the ROMAP data, which revealed a triple bounce, leading the lander to its final landing site (Abydos area). This location was narrowed down to an area of $150 \times 15\ m^2$, using CONSERT for ranging, but the visual contact with Philae was lost. One of the images shows the "footprints" at the first contact with the comet surface (Fig. 9) and another shows the dust cloud produced by the impact. The rotation and attitude of Philae have been inferred from ROMAP magnetometer data, solar generator housekeeping values, MUPUS-TM sensor and thermal reference sensor data and system temperature sensors. On November 15, 2014, 00:07, Philae entered "hibernation" when the lander voltage dropped below the threshold for operations.

4.2 Philae panoply

The Rosetta lander was the first spacecraft ever to make a soft landing on the surface of a comet nucleus. The lander was provided by a European consortium (DLR, ESA, CNES and scientific institutes from Austria, Finland, France, Hungary, Ireland, Italy and the UK). The Lander structure consisted of a baseplate, an instrument platform and a polygonal sandwich construction, all made of carbon fiber. Some of the instruments and subsystems were beneath a hood covered with solar cells. Data were transmitted from the comet surface to Earth via the orbiter. The Philae lander carried ten instruments for in situ analysis:

- the Alpha Proton X-ray Spectrometer (APXS) to study the chemical composition of the landing site and its potential alteration during the comet's approach to the Sun (Klingelhöfer et al. 2007);

- the Comet nucleus Infrared and Visible Analyzer (CIVA) composed of six mini-cameras to take panoramic pictures of the comet surface (Bibring et al. 2007);
- the COmet Nucleus Sounding Experiment by Radiowave Transmission (CONSERT) to study the internal structure of the comet nucleus. Instrument components were on both the orbiter and the lander, to establish a radio link that passes through the comet nucleus. The way in which the radio waves propagate through the nucleus gives scientists clues of its structure and nature (Kofman et al. 2007);
- the COmetary SAmpling and Composition Experiment (COSAC), is an evolved gas analyzer composed of a multi-column gas chromatograph (GC) coupled to a linear reflectron time-of-flight mass-spectrometer and aimed to detect and identify complex organic molecules (Goesmann et al. 2007);
- PTOLEMY (Wright et al. 2007) is a gas sampling device for the analysis of stable isotope ratios at high precisions and accuracies, the target isotope ratios being $^{12}C/^{13}C$, $^{14}N/^{15}N$, $^{16}O/^{17}O$, $^{16}O/^{18}O$ and D/H, using the Methods Of Determining and Understanding Light elements from Unequivocal Stable isotope compositions (MODULUS, Wright and Pillinger 1998);
- theMUlti-PUrpose Sensors for Surface and Sub-Surface Science (MUPUS) is a thermal probe hammered into the regolith of the comet nucleus (up to a depth of 32 cm) aimed to study the temperature profile, the thermal diffusivity and conductivity profiles underneath the surface; moreover, the mechanical strength of the nucleus material is derived from the energy spent per unit distance penetrated during the insertion (Spohn et al. 2007);
- the ROsetta Lander Imaging System (ROLIS) during Philae's descent provided a far field (from an altitude of 3300 m) and a near field sequence (from 67.4 m to 9 m) of close-up images of the landing site at a resolution increasing from 3.3 m px^{-1} to 0.95 cm px^{-1} (Mottola et al. 2007);
- the ROsetta Lander MAgnetometer and Plasma Monitor (ROMAP) measure the magnetic field of the comet with a fluxgate magnetometer, and the near nucleus plasma environment with one electron and two ion spectrometers (Auster et al. 2007);
- the Sampling, Drilling and Distribution (SD2) subsystem is a drilling device capable of collecting samples up to 23 cm depth and delivering material to onboard instruments for analysis (Ercoli-Finzi et al. 2007);
- the Surface Electric Sounding and Acoustic Monitoring Experiment (SESAME) is a threefold instrument composed of the Comet Acoustic Surface Sounding Experiment (CASSE), the Dust Impact Monitor (DIM) and the Permittivity Probe (PP) aimed at measuring the mechanical and electrical parameters of the comet (Seidensticker et al. 2007).

Though the Philae landing was not nominal, all the onboard instruments were switched on after the first touchdown (TD1) and collected precious in situ data to characterize the main properties of the P67 surface.

4.3 Philae results

During the descent, ROLIS took several images of the surface at the Agilkia site, toward which Philae was directed (Mottola et al. 2015). These images reveal a surface covered by a regolith layer having variable thickness (from 0 up to 2 m) and composed of debris and boulders (whose size range is from cm to m). There are two different kinds of terrains, one rougher with a coarse regolith layer and the other smoother with much less decimeter-sized blocks. At 1 cm px^{-1} resolution, the surface appears granular, without any apparent dust deposits, though the presence of material deposits (similar to wind tail features) indicate possible erosion processes and material displacement, driven by particles pushed by the comet's activity.

Signals that were received by CONSERT on Rosetta from Philae during the two nominal periods of measurements propagated through parts of the nucleus and are as narrow as the calibration signal (see Fig. 10).

No signature of volume or surface scattering effects are present in these signal forms: the medium swiped by the waves is rather homogeneous and/or that the dielectric behavior between possible inclusions inside the nucleus (different in composition and porosity) is similar. This implies that the upper part of the "head" of 67P is fairly

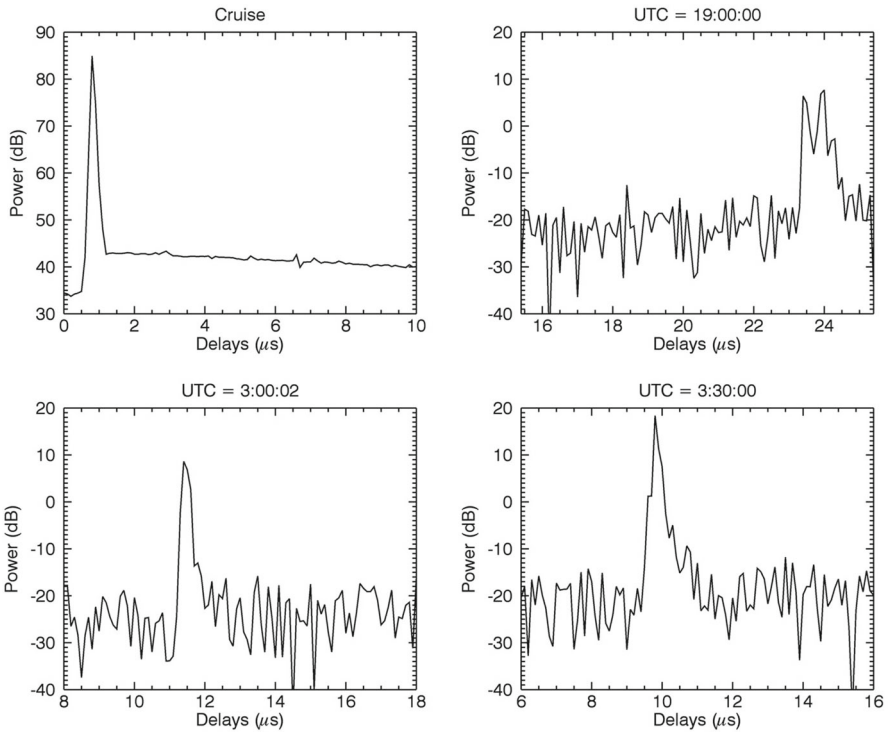

Fig. 10 Signals obtained by CONSERT that have propagated through the nucleus, as measured at the output of the matched filter, are presented for different measurement times and compared with the calibration signal during the cruise phase (adapted from Kofman et al. 2015)

homogeneous on a spatial scale of tens of meters. The average permittivity is about 1.27, suggesting that this region has a volumetric dust/ice ratio of 0.4 to 2.6 and a porosity of 75 to 85%. The dust component may be comparable to that of carbonaceous chondrites (Kofman et al. 2015).

Lethuillier et al. (2016) measured the dielectric constant of the first meter below the surface at Abydos (see Fig. 15) obtaining a value $> 2.45 \pm 0.20$, which is consistent with a porosity $< 50\%$ if the dust phase is analogous to carbonaceous chondrites and $< 75\%$ in the case of less primitive ordinary chondrites. This indicates that the near surface layer of the nucleus of 67P seems to be more compact than its interior and suggests that it could consist of a sintered dust–ice layer.

On the basis of magnetic field measurements during the descent and subsequent multiple touchdown of Philae, no global magnetic field was detected by ROMAP (Auster et al. 2015). An upper magnetic field magnitude < 2 nanotesla was measured by ROMAP at multiple locations of the comet surface. The maximum dipole moment of 67P is 1.6×10^8 Am^2.

The mechanical response of Philae's structure elements at the multiple touchdown in Agilkia and TD2 sites and at its final position in Abydos has been analyzed by Biele et al. (2015). These authors, combining a numerical multibody model of Philae with a soil mechanics force model to determine the comet soil properties, provide a tentative mechanical model of the upper surface layers as follows. At Agilkia, the surface is composed of granular and soft regolith layer (compressive strength of ~ 1 kPa) thick ~ 20 cm with small (≤ 1 cm) particle sizes, whose distribution is still granular at 0.9 cm px^{-1} and is interpreted as "air fall" (Thomas et al. 2015a), so that the whole region appears to be covered by a smooth "dust" layer. Abydos and TD2 sites expose a consolidated surface with few boulders, hard and stiff with a (crushing) strength of at least 2 MPa, possibly part of the basal unit. This layer may be similar to the possible subsurface layer at Agilkia. These values were confirmed by the fact that the MUPUS thermal probe did not fully penetrate the near-surface layers and from the records of the MUPUS-PEN hammering onto the surface, a local resistance of the ground to penetration of > 4 megapascals, equivalent to > 2 megapascal uniaxial compressive strength, has been estimated (Spohn et al. 2015). The diurnal temperature at Abydos varied between 90 and 130 K, the surface emissivity was 0.97, and the local thermal inertia was 85 ± 35 J m^{-2} K^{-1}s$^{-1/2}$. These data suggest that the nucleus has a low thermal conductivity and is a highly porous body with a sub-surficial dust–ice sediment with locally substantial compressive strength.

The surface material imaged by the CIVA panoramas (Fig. 11) in the close surroundings of Philae shows different structures and brightnesses, with two end members.

The first consists of agglomerates of dark (pristine?) accreted granular material, with grain size in the millimeter-to-centimeter range, dominated by carbon-rich species. Several pebble-like grains seem loosely attached to the surface, possibly resulting from a re-deposition process which could have originated from rough consolidated terrains. The second end member is characterized by brighter grains and decametric-scale areas with smoother texture. The great number of fractures and cracks, probably resulting from thermal stress, are at the origin of the fragmentation and the erosion of the comet surface (Bibring et al. 2015). Poulet et al. (2016) derived quantitative analysis of the fractures and pebbles visible in the CIVA-P images (Fig. 12). Fragmentation

Fig. 11 The CIVA-P panorama images (ESA/Rosetta/Philae/CIVA)

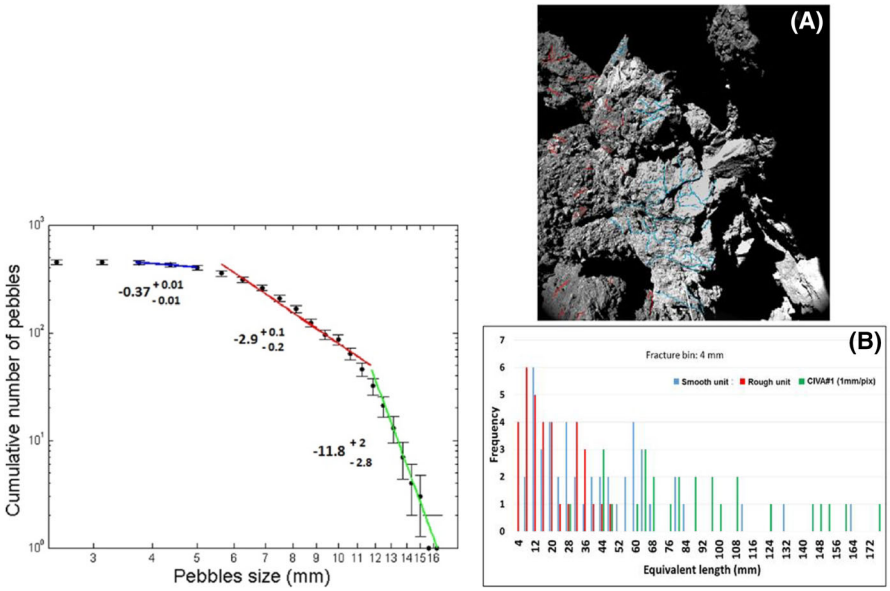

Fig. 12 Left: cumulative size–frequency distribution of pebbles larger than 6 CIVA pixels (3.7 mm). Right: **a** map of the fractures on a CIVA image. The fractures observed in the smooth unit are in blue, while those in rough/granular unit are in red. **b** Histogram of frequency versus fracture lengths of the three major lithologies (adapted by Poulet et al. 2016)

by thermal insolation and/or loss of volatiles is a possible mechanism to explain the features observed by CIVA and they speculated that the pebbles are remnants of primordial accretion processes.

These observations have been complemented by six images of the surface below the lander, acquired by ROLIS with a resolution of 0.8 mm per pixel (Schröder et al. 2017). These images (four of which were illuminated by the camera LEDs of different

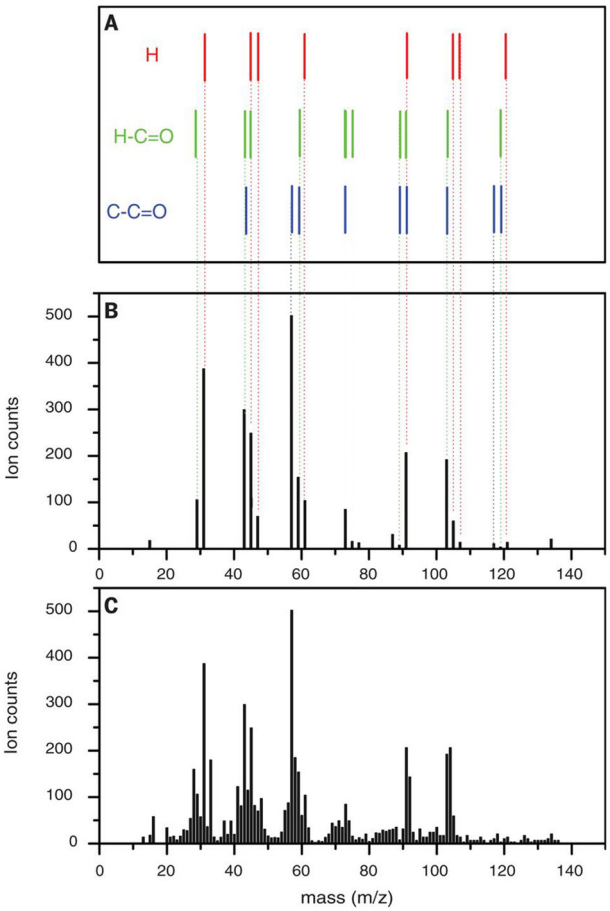

Fig. 13 The proposed polyoxymethylene fit to the Ptolemy spectra. **a** Schematic for the proposed mass fragments of polyoxymethylene with different terminations. **b** Peaks that are considered to be from polyoxymethylene. **c** Ptolemy spectra with peaks from H_2O and CO_2 removed (from Wright et al. 2015)

colors) confirm that Philae was perched on a sloped lumpy surface that seems to consist of smooth, cracked plates with unconsolidated edges.

The determination of chemical composition of the nucleus surface by "in situ" measurements has been heavily affected by the Philae landing sequence and its final setting. The two mass spectrometers, Ptolemy and COSAC, took data some minutes after the first TD, obtaining different results because Ptolemy sampled mostly coma gases entering exhaust tubes located on top of the lander pointing toward the sky, while COSAC sampled essentially dust particles excavated by the impact that entered the warm exhaust tubes located on the bottom of the lander, pointing toward the surface. Ptolemy operating in "sniff mode" obtained a mass spectra during the first contact with the comet (Fig. 13). The chemical composition of the surface reveals a complex mixture of organics, H_2O and CO_2. Wright et al. (2015) suggest the presence of polyoxymethylene $(CH_2O)_n$ to interpret many of the features of the mass spectra,

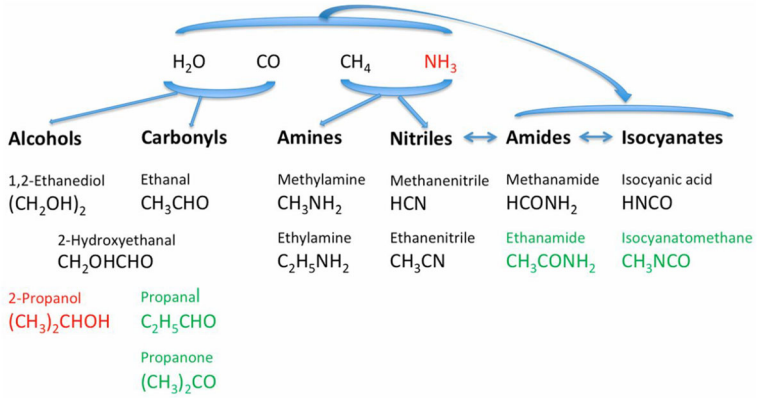

Fig. 14 Possible formation pathways of COSAC compounds. Species in red are not confidently identified, while species in green are reported for the first time in a comet (from Goesmann et al. 2015)

together with other compounds at low concentrations. The presence of this compound could provide an explanation for the presence of observable formaldehyde in cometary coma.

COSAC gas spectrum displayed a suite of 16 organic compounds, some of which were detected for the first time in a comet (Goesmann et al. 2015), forming a consistent set related by a plausible formation scheme (Fig. 14), if a nitrogen source such as NH_3 were originally abundant enough to form the found N-bearing species, which have since been lost (evaporated or used up in reactions). Such a complexity of the cometary chemistry suggests that the formation of prebiotic material was favored by the early solar system chemistry.

4.4 Philae found

A multi-instrument collaboration was set up to obtain the location where Philae was hidden. The radar data collected from the CONSERT were used to triangulate Philae's location to the general area; images taken by CIVA helped in identifying key features of the final landing terrain. Moreover, the radio links between Rosetta and Philae during the periods when Philae was receiving/transmitting and the Sun illumination data received from the lander solar panels yielded "line-of-sight" information, because no obstacles were interposed between Philae and Rosetta or Philae and the Sun. During all mission opportunities when the probe was within 20 km of the nucleus, the OSIRIS cameras were engaged in a search of the lost lander.

The final search was carried out from March 2016 up to the beginning of September 2016. The spots to look at have always been chosen within CONCERT's hypothetical landing sites taking images from different viewing angles around the comet: (1) to avoid that a rock blocks the lander from been seen from one direction, while it would remain visible from another; (2) to take advantage of different illumination conditions and phase angles. Many candidate sites were discarded one after the other because the images revealed their natural features (ice spots, brilliant boulders, etc.). One of

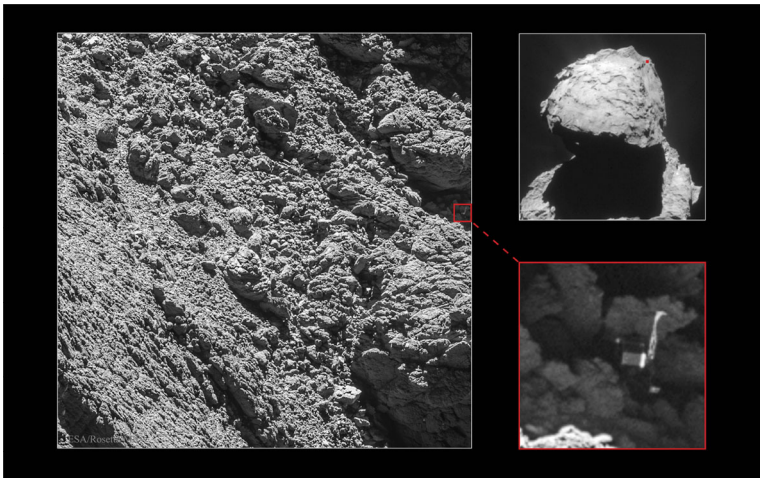

Fig. 15 After some 22 months since it landed, Philae was spotted on the far right-hand side of an image taken on September 2, 2016. The Philae lander is seen on the far right of the left main image in a shadow area, with insert images showing a zoom out. Credits: ESA/Rosetta/MPS for OSIRIS Team MPS/UPD/LAM/IAA/SSO/INTA/UPM/DASP/IDA

the best candidate sites was always hidden to the views of the OSIRIS cameras by a nose rock, but at the last available slot of observations, on September 2, Rosetta's field of view allowed the camera to take high-resolution images—5 cm px^{-1} over the very front edge of the nose rock at a distance of 2.7 km from the surface (Fig. 15). On September 4, members of the OSIRIS team, studying the images downlinked to Earth and searching in the position under the cliff where the spacecraft was pointed, finally found Philae in the corner of the image (Fig. 15).

5 The living comet

5.1 Shape and surface morphology

Starting on March 23, 2014 when the spacecraft was at a distance of 5 million km from the comet and all along the Rosetta mission, the OSIRIS camera imaged the comet 67P/Churyumov–Gerasimenko with the 25 filters covering from 240 to 1000 nm. The NAC camera resolved the nucleus (>1 pixel) on June 16, 2014 when the spacecraft was at a distance of 192,000 km up to a resolution down to 10 cm px^{-1} during closer encounters and even lower during the final Rosetta landing phase.

From September 2014 with a resolution of 0.8 m px^{-1}, the shape of the comet nucleus was well defined with two lobes in contact. The complete map of the comet was obtained when the spacecraft was close to the perihelion passage on August 2015. The comet showed an irregular shape like a "duck" with two distinct parts: the large one (called the body) with a size of $4.10 \times 3.52 \times 1.63$ km^3, and the small (called the head) with a size of $2.50 \times 2.14 \times 1.64$ km^3 (Jorda et al. 2016). The spin axis is prograde with coordinates of RA $= 69.3° \pm 0.1°$ and dec $= 64.1 \pm 0.1°$ and a

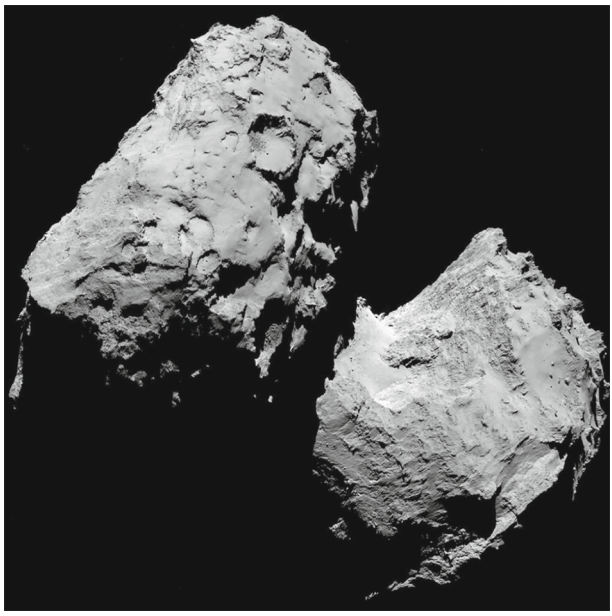

Fig. 16 Image taken by OSIRIS NAC on August 8, 2014 when the spacecraft was at an altitude of 111 km with a spatial resolution of 2 m px^{-1} (ESA/Rosetta/MPS for OSIRIS Team MPS/UPD/LAM/IAA/SSO/INTA/UPM/DASP/IDA)

rotational period of 12.4043 ± 0.0007 h (Sierks et al. 2015). The volume of the two lobes corresponds to 66% and 27%, respectively, of the total volume of the nucleus. A neck connects the two lobes with an estimation of about 7% of the total volume of the comet nucleus. A total volume of 18.8 ± 0.3 km^3 has been computed and combining with the mass determined by Radio Science investigation of 9.982 ± 0.003 × 10^9 kg (Patzold et al. 2016), a mean density of 532 ± 7 $kg\,m^{-3}$ was calculated. This density implies a large value of porosity of 70–80% with an ice/dust mixture assumed to have a density of 1500–2000 $kg\,m^{-3}$. The peculiar shape of the comet shows also a surface characterized by complex morphology including a large variety of terrains (Sierks et al. 2015) and a mean geometric albedo of 6.5 ± 0.2% at 649 nm (Fornasier et al. 2015) with local variations (Fig. 16).

The numerous images (about 80,000 obtained during the entire mission) showed a comet with a morphological complex surface with different terrain types and numerous intricate features, which imply a variety of processes. The complete surface was divided into 26 regions (Thomas et al. 2015a, b; El-Maarry et al. 2015, 2016), defined based on large-scale boundaries. The regional boundaries were chosen to discriminate the surface in distinctive regions on the basis of their morphological and/or topographical properties. These regions were named after ancient Egyptian deities, in accordance with the general theme of the Rosetta mission in using ancient Egyptian names. In Fig. 17, the regions in different colors are reported with their relative names.

The 26 different regions can be grouped into five basic categories: dust-covered terrains, brittle materials with pits and circular structures, larger-scale depressions, smooth terrains and exposed consolidated surfaces.

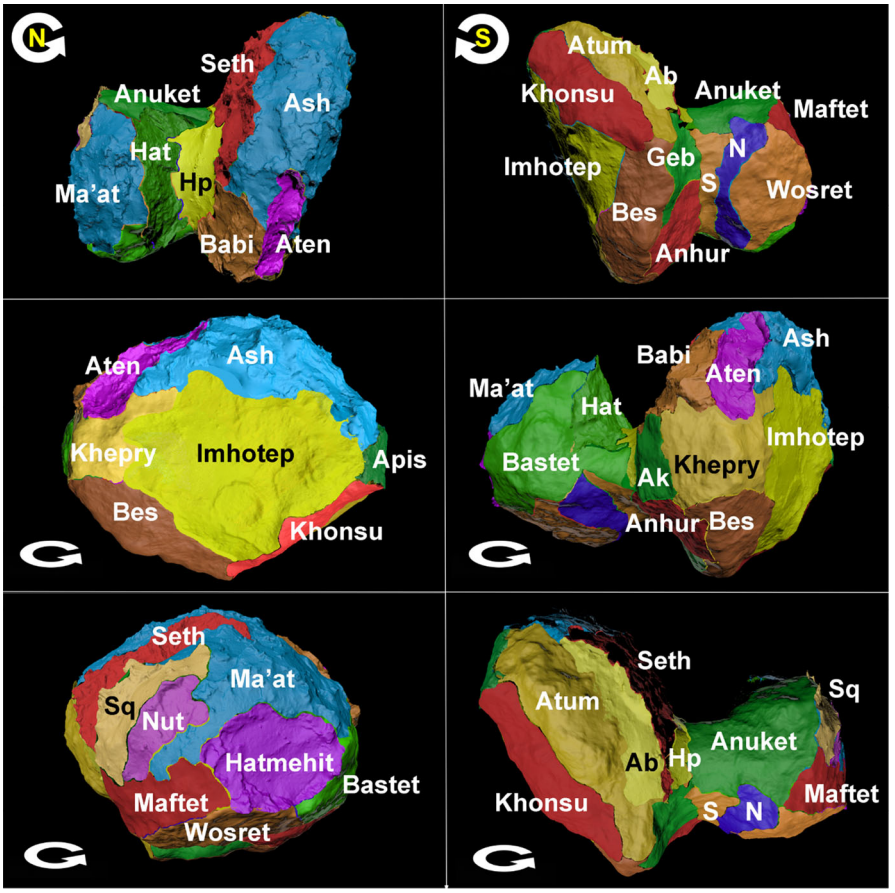

Fig. 17 The 26 geological regions identified on 67P/C-G are reported in the images acquired by the OSIRIS camera, showing the northern and southern hemispheres of comet 67P/Churyumov–Gerasimenko, from El-Maarry et al. (2016). *Ab* Anubis region, *Ak* Aker, *Hp* Hapi, *N* Neith, *S* Sobet, *Sq* Serqet

"Dust-covered terrains" are regions which appear coated with smooth covering of dust such as Ma'at, Ash and Hapi regions. These terrains are characterized by materials showing signs of widespread mobilization and revealing outcrops of underlying units. The dust is created by activity that produces low-velocity non-escaping dust particles. The thickness is variable and uncertain. Dune-like structures are also evident on data taken at high resolution that could be the result of eolian-driven surface transport of the dust (see Sect. 5.2 for further description).

The regions with "brittle material" show evidences of fracturing and collapse of this material with mass wasting stratum. The surface is covered by weakly consolidated materials showing signs of mechanical failure and gradually evolving into talus-like deposit. The evidence of collapse and the low gravity of the body indicate low tensile strength. Seth and Imhotep regions show evidence of consolidated brittle material. Several circular and steep-walled depressions also dominate the Seth region.

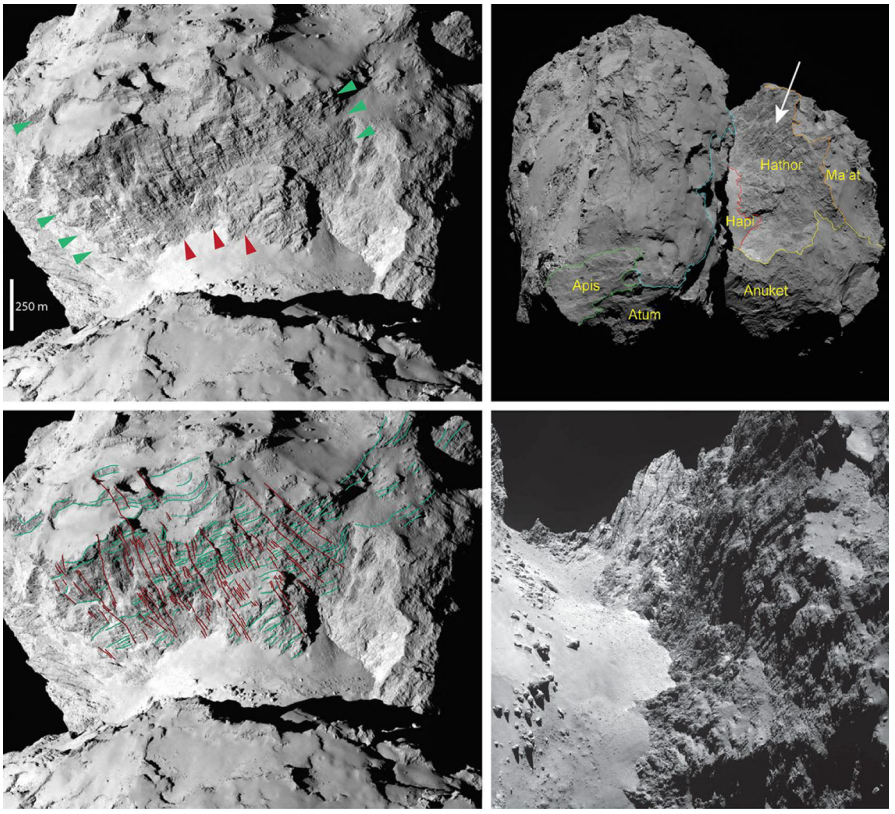

Fig. 18 Different Hathor images taken by the NAC camera (Thomas et al. 2015a, b). The region is characterized by 900 m high "cliff" which rises up from the Hapi region. A set of lineaments and fractures are vertical along the cliff with some perpendicular lineaments aligned with small terraces, indicating inner layering (ESA/Rosetta/MPS for OSIRIS Team MPS/UPD/LAM/IAA/SSO/INTA/UPM/DASP/IDA)

"Large-scale depression structures" exist in the head and in the body of the nucleus. A circular depression of 1 km in diameter represents the Hatmehit region on the head of the nucleus. The depression structure in the body is called Aten and it is surrounded by the brittle material of Ash. The interior of Aten is covered with boulders. It has been suggested that Aten has been formed by one or more major mass loss events.

"Smooth terrains" refers to units that generally appear to be composed of non-cohesive materials enclosed by rough consolidated units and are particularly thick enough to mask the underlying units. These terrains are representatives of areas like Imhotep, Anubis and Hapi, which are characterized by extremely smooth material. The Imhotep region (see Fig. 19) is dominated by a smooth area that covers more than 0.7 km^2, and this smooth material is surrounded on three sides by fractured consolidated material. Smooth terrain is seen at several topographic levels in the region. The Anubis region is similar to Imhotep, but without circular structures. The Hapi region is completely different from the other two and is formed by smooth material piled up against the faces of Hathor and Seth, suggesting that particles are falling back from these faces (see Fig. 18).

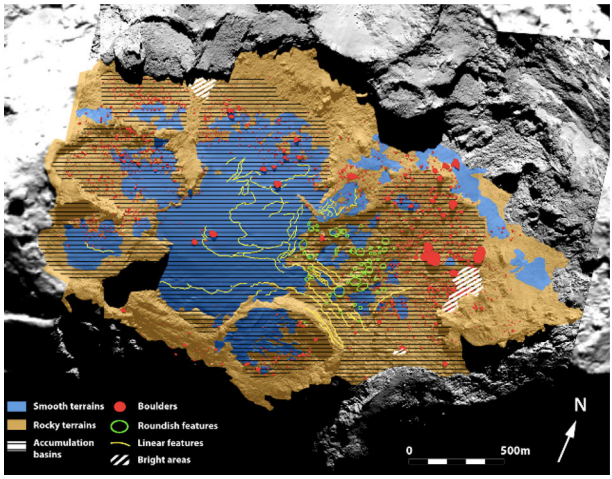

Fig. 19 Geomorphological map of the Imhotep region as reported by Auger et al. (2015). The main geological features are reported with different symbols

The regions with "exposed consolidated terrains" refer to units that appear rocky and are cohesive enough to display lineaments and fractures even if their density is much lower than any terrestrial rock. The consolidated terrains represent the most common region type on both lobes. One of the most typical areas is Hathor which consists of a 900 m high "cliff" characterized by a set of aligned linear features (Fig. 18). Anuket, which borders Hathor and is part of external surface of the head, has also consolidated surface and contains some cracks which are parallel to the neck. The Aker region, on the body, contains consolidated material as well a set of fractures larger than 200 m in length. Many linear features are present in the Aker region and on a large part of the neighboring Khepry region. It is possible to observe the consolidated materials even in dust-dominated and smooth regions. Most of the very consolidated terrains show different degrees of fractures with various orientations, irregularity or polygonal shape. The presence of fractured materials on the surface of the comet that has a very low bulk density could indicate some heterogeneity of some physical parameters such as porosity and/or composition within the comet.

The bi-lobed shape was carefully analyzed to understand the origin of the comet and whether it was two distinct objects or the shape was the result of localized excavation on the outgassing region in the area between the two lobes. The surface structure of the body (major lobe) of the comet is enveloped by a continuous set of layers, of depth up to 650 m, which seems completely independent of the layers that envelope the head (minor lobe). All regions of the main body are characterized by layering (like an onion) and/or terraces, with the exception of the Aten region which is a depression covered by debris material (Massironi et al. 2015). The spectacular region Hathor covers about one-third of the head inner structure with dimensions of about 900 m high and 1500 m wide. Hathor cliff is formed by regular layering, which is crosscut by perpendicular lineaments and small terraces.

5.2 Geology and surface processes

The surface of the comet shows a large variety of geological structures. The "head" is characterized by cliffs and linear structures larger than 500 m. Many cracks (El-Maarry et al. 2017) are present in particular on the surface of the neck. Many peculiar features are also present with steep slopes called "goosebumps". The Imhotep region (Fig. 19) is one of the most interesting areas showing a variety of features. Auger et al. (2015) described the geology of the region by dividing it in two different terrains, smooth and rocky, and with three different morphological features: linear, roundish and boulders. In the smooth terrains, the surface is consistent with relatively fine grains with inhomogeneity in the size distribution for the largest one. These smooth terrains cover one-third of the Imhotep region. The rocky terrains are with more consolidated material and are made with highly fractured material. The roundish features are characterized by circular, elliptical or irregular roundish shapes elevated with respect to the surrounding. The accumulation basins are areas where the fine material and boulders seem accumulated. The linear features are from hundreds of meters up to 1 km. The boulders are of different size up to 90 m and different in texture and can be conglomerate or highly fractured.

Temporal variations were detected all around the surface of the comet; particularly spectacular changes have been observed in the Imhotep region. Starting from end of May 2015, Groussin et al. (2015) observed a roundish feature appearing in the Imhotep region and expanding in the following days. Several features appeared with dramatically changing morphology in about 1 month, changing for more than 40% the surface of this area. Many bluish materials appeared on the surface. From the spectrophotometric analysis, these terrains appear almost with neutral (flat slope) spectra in comparison to the average spectral slope of the nucleus, which is about 16% per 100 nm. This blue material has been suggested to be associated with ice by Fornasier et al. (2015) and Pommerol et al. (2015) and confirmed by VIRTIS data (Filacchione et al. 2016a; Barucci et al. 2016). The fresh material is hidden by dust deposit that has been removed by the erosion processes. This is also in good agreement with the low thermal inertia of 10–50 JK^{-1} m^{-2} $s^{-0.5}$ of the nucleus surface determined by VIRTIS (Capaccioni et al. 2015) and MIRO instruments (Gulkis et al. 2015). OSIRIS images observed in the same area a collapse of the upper surface (about 5m). This was observed starting on scarps, cliffs or edges where the seasonal heating reaches the underlying volatile-rich materials. These variations, observed in May–July 2015 by Groussin et al. (2015), moved away from the scarps and cliffs which are composed of consolidated materials and consequently more difficult to erode. During the period of the erosion process, a part of the dust particles fall and accumulate at the foot of the expanding features or are transported far away.

Starting in March 2015, the southern hemisphere of the comet began to be visible, coming out from its long winter and going to the strongest heating and high erosion period, thus exposing the more fresh, pristine material. Some regions are very peculiar, such as Anhur and Khonsu. Anhur appears strongly eroded with elongated canyon-like structures, scarp and different kinds of deposits. Fornasier et al. (2016) discovered a large area rich in H_2O ice (1500 m^2) appearing and then disappearing after 10 days. Thin frosts sublimating in some minutes were also observed close to the shadows.

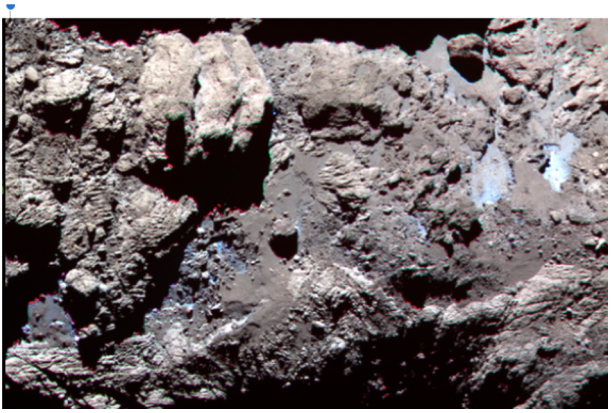

Fig. 20 An RGB mage of the Khonsu region. The red, green and blue images correspond to the OSIRIS NAC at the respective filters: 882.1, 649.2 and 480.7 nm. The red features near the shadow are artifacts due to the co-registrations of the images

Khonsu displays both smooth and rough terrain with a large quantity of boulders and irregular outcrops (Fig. 20). It is characterized by a number of irregularly shaped outcrops and a high number of large boulders (many exceeding 30 m in diameter). One of the most remarkable features in this region is a 200 m-wide composite block of material that appears to be arranged in a stack of three plate-shaped features (like a "pancake"). The Khonsu region started to be freshly exposed to the sun and showed prominent bright spots (Barucci et al. 2016; Deshaprya et al. 2016) varying with time. These cyclic processes are spread on the comet and lead to continuously varying surface properties.

The presence of all these different structures suggest that surface dust transport is important in the uppermost surface layer of numerous regions. Surface deposit are also evident in many regions on the nucleus. The source of the dust is activity that produces low-velocity non-escaping dust particles in the form of airfall. Thomas et al. (2015a, b) showed the evidence for motion material from one side to another and demonstrated that "airfall", as a consequence of non-escaping particles emitted, could be a plausible explanation for the smooth deposits. In the deposits, there are also bright chunks of material which could be associated with water ice. Rotundi et al. (2015) provided evidence of slow-moving particles in bound orbits around the nucleus, which may either escape or impact the nucleus surface. The presence of dune-like structures has been identified on the surfaces of these deposits. Some eolian-like ripples (regular patterns) are evident in several regions as in the Hapi region with a field width of about 60 m (Fig. 21). They may be the result of eolian-driven surface transport of the dust generated by local sublimation. The dominant forces of these ripples are different from those seen elsewhere in the solar system. To initiate saltation, the surface shear stress from the gas expansion of a vent must overcome the gravitational force and interparticle forces.

Many pits have been also observed (Vincent et al. 2015) on the surface of 67P which seem clustered in groups with several active pits (see Fig. 22). Pits have been detected also in other comets and it has been argued that they can represent signatures

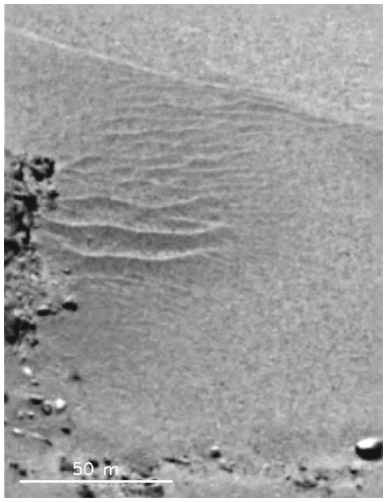

Fig. 21 Eolian-like ripples in the Hapi region on 67P. Image taken by NAC on 17 September 2014 (Thomas et al. 2015b)

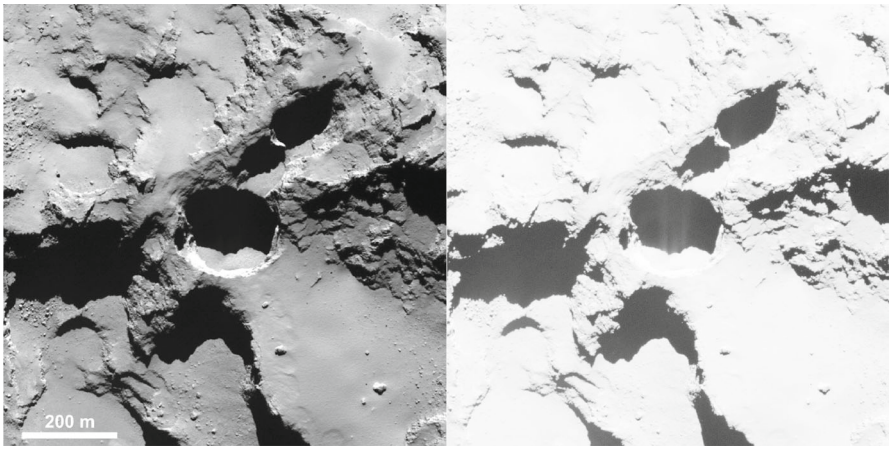

Fig. 22 Close-up OSIRIS image of a large pit (at left) at 60 km from the comet's nucleus. The contrast of the image (at right) has been stretched to reveal the details of the fine structure with a clear jet from the pit's interior (ESA/Rosetta/MPS for OSIRIS Team MPS/UPD/LAM/IAA/SSO/INTA/UPM/DASP/IDA)

of endogenic activity. The terrains inside the pits are very different with smooth texture, fractures, terraces and alcoves or globular texture. The walls, extending to 100 m, show linear structures that are parallel to their floors. The cylindrical shape of most of the pits provides evidence against formation by erosion. Vincent et al. (2015) suggested that pits could be created by sinkhole process and possibly accompanied by outburst and therefore pits could characterize how the surface evolved or was fresh. The distribution and the dimension of the pits imply a large heterogeneity on the physical, structural and compositional properties of the few 100 m below the observed surface. Clusters of pits as well as collapsed structures are signatures of the thermal history of the comet.

Pits were also observed in great detail during the final controlled Rosetta impact on the Ma'at region on September 30, 2016. This target area was chosen because of being rich in several active pits measuring over 100 m wide and 60 m deep. The final image shows the regolith surface with a resolution up to 2 mm px^{-1}.

Between the different and rich geological features characterizing the surface of the comet, boulders of various sizes have been observed. These type of features are typical on asteroids or satellites, but it is the first time that they have been observed on a comet. The size–frequency boulder distribution per km^2 was measured by Pajola et al. (2015, 2016a, b) on the entire surface of the comet. The results show that there is an overlap of the slope of cumulative distributions between the body and the head. The similar power-slope index suggests that similar boulder formation processes occur in both hemispheres. The difference with the neck is much higher, suggesting that the numerous boulders located on the neck region are the results of the boulders falling from the contiguous Hathor cliff (see Fig. 18). Similar cumulative size distributions have been observed when there are similar geomorphological properties. This suggests that similar activity processes, pit formation, thermal fractures or gravitational collapses occurred in different areas of the comet, forming the size–frequency distribution observed today. Several effects connected by sublimation can be associated with the neck distribution observed, such as disintegration or fragmentation, uplifting and production of dust blanket covering the small boulders. Larger number of boulders per km^2 have been counted in the southern hemisphere in comparison to the northern one (about a factor 3), suggesting a stronger sublimation activity on the southern area of the comet. Thermal fracturing, erosions and gravitational events could be the cause of the greater production of boulders.

Many jets have been observed from the comet and connected with morphological structures and changes of the surface. Outbursts have also been observed (Vincent et al. 2016b) and suggested that they could be provoked by collapsing cliffs. Pajola et al. (2017), observing the Aswan region, detected a new outburst just few days after a plume detection near the collapse of the cliff, showing the first clear evidence that the observed outburst was directly linked to the collapse of the cliff. The collapse revealed fresh ice from the interior at high albedo, forming a new talus. Diurnal thermal gradients, as well as seasonal variations may have driven cyclic and cumulative opening of such fractures. The collapse of the Answan cliff makes it the first landslide to have been observed on a comet. On the 67P, multiple taluses have been detected and associated with cliffs suggesting that cliff collapses are important processes which reshape the comet surface. The erosion history of the comet is very important and depends on the dynamical age connected with the followed orbits. It gives constraints on the evolution history of the comet.

5.3 Activity

The comet 67P/Churyumov–Gerasimenko was selected as a target of the Rosetta mission because of its low activity level, providing a less dangerous environment for the spacecraft. The activity is at the origin of the coma, which constitutes a gaseous and a dusty component. The increasing warmth from the Sun causes surface ice to

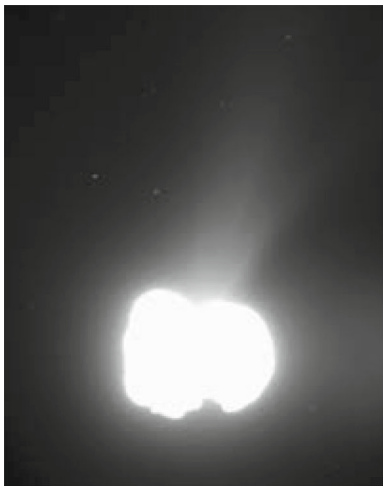

Fig. 23 An overexposed image of Comet 67P/Churyumov–Gerasimenko, taken 550 km away, revealing the location of activity on 2 August 2014 (ESA/Rosetta/MPS for OSIRIS Team MPS/UPD/LAM/IAA/SSO/INTA/UPM/DASP/IDA)

sublimate and the gas escapes from the rock–ice nucleus. As the cloud of gas flows away from the nucleus and out into space, it also carries dust particles: together, these slowly expand to create the coma (Fig. 23).

Since the first images at the end of April 2014, thanks to the OSIRIS camera, it was possible to observe one outburst and detect dust in the coma. Starting from July 2014, when the comet was at 3.7 AU from the Sun and the spacecraft at a distance of 3000 km, OSIRIS detected and resolved features in the coma. The neck, the transition region between the head and the body parts of the comet, was the most active area, while minor activity was detectable from both lobes of the comet.

The comet has a heterogeneous coma dominated by large fluctuations in composition with important diurnal and seasonal variations in the major outgassing species H_2O, CO_2 and CO (Hassig et al. 2015), indicating complex coma–nucleus relationship. The observed variations in the coma are also the consequence of the nucleus shape coupled with the obliquity of its spin: in fact, the gas density in the coma is strongly affected by (1) the nucleus concavities, even if the distribution of ices on the nucleus surface is quite uniform (Bieler et al. 2015a) and (2) the nucleus sunlit area varies by more than a factor of 2. Lee et al. (2015) show that the amount of water-outgassing rate changes from 0.1 to 3×10^{25} molecules $s^{-1}sr^{-1}$, with gas expansion velocities in the range of 0.61–0.78 km s^{-1}, and terminal gas temperatures from 47 to 74 K. Moreover, analyzing the $H_2{}^{16}O$ and $H_2{}^{18}O$ (110–101) lines, Biver et al. (2015) found that at a distance > 3 AU the water column density varies by two orders of magnitude. The highest value came on the dayside from a region close to the neck, suggesting that these areas are the most productive in water vapor, while the lowest value is observed against the nucleus nightside corresponding to a very low outgassing. Part of the variation of the outgassing activity is thus determined by the diurnal cycle, depending on the effective local solar time of the day, i.e., the outgassing activity diminishes abruptly after the local sunset time. It also indicates that the sublimating ice is located within a depth of 1–2 cm in the diurnal thermal layer (Gulkis et al.

2015). The seasonal variations could be the effects of differences in the subsurface temperature in the nucleus (Hassig et al. 2015).

Alice UV spectrometer detected emissions of atomic hydrogen and oxygen (Feldman et al. (2015). These emissions are enhanced above the comet's neck. Weaker emissions from atomic carbon were also detected and the relative brightness to HI reflects the variation of CO_2 to H_2O column abundance in the coma. The far UV emissions of H, O and C atoms were expected, since they have been observed many times in comets, as a result of resonance scattering of solar photons on these atoms, produced from photo-dissociation of H_2O and CO_2. However, ALICE explored regions near the nucleus (a few km) never observed before, where the UV emission process is different: H_2O and CO_2 molecules are destroyed by electron impact, and H, O and C atoms are produced in an excited state and de-excite with the corresponding UV emission. Therefore, these emissions trace directly the distributions of H_2O and CO_2 in the coma.

The global water production remained quite constant from 2.9 to 2.5 AU and the CO_2/H_2O column density ratio varied from 2 to 60% (Bockelée-Morvan et al. 2015). $CO_2$was outgassing from both illuminated and non-illuminated regions, implying that CO_2 sublimated from below the diurnal thermal layer. A general large-scale anti-correlation can be observed between H_2O and CO_2 (Mall et al. 2016). CO and CO_2 are more abundant than in other Jupiter family comets, while nitrogen is depleted, as indicated by the low values of N_2 and of the typical N-bearing species. Bieler et al. (2015b) report the detection of abundant O_2 in the coma of comet 67P (abundances in the range 1–10% relative to H_2O and mean value of 3.80 % $\pm$ 0.85). The O_2/H_2O ratio is isotropic in the coma and does not change with heliocentric distance, suggesting that primordial O_2 was incorporated into the nucleus during the comet's formation.

Since the first in situ measurements, Le Roy et al. (2015) detected many volatile species in the cometary coma, whose relative abundances are different between the summer and winter hemispheres. Coma heterogeneity is not limited to the major outgassing species. Minor species show better correlation with either H_2O or CO_2. The molecule CH_4 shows a different diurnal pattern from all other analyzed species. Ethane is abundant in the southern hemisphere. Such features have implications for nucleus heterogeneity and thermal processing (Luspay-Kuti et al. 2015).

The water production rate measured by the various Rosetta instruments (ROSINA DFMS and COPS, MIRO, VIRTIS-H and RPC/ICA) over the period spanning 4.0 AU inbound to 2.7 AU outbound is presented in Fig. 24 (Hansen et al. 2016). Beyond 3.5 AU, the water production did not increase with decreasing heliocentric distance as expected. At the time of the inbound equinox, the maximum water production passed from the north to the south and, as Fougere et al. (2016) claim, for a rapid transition of the averaged production over a comet rotation from a peak at $\sim 55°$N to $\sim 50°$S. At perihelion, there is some evidence of two or three time-dependent increases in the water production. The peak of water production occurs about 20 days after perihelion with peak production of $(3.5 \pm 0.5) \times 10^{28}$ molecules s^{-1}. The heliocentric dependence of the water production is represented by two power laws: all the data collected before the perihelion are fitted by a power law with exponent -5.3 and those coming after the perihelion by a power law with exponent -7.1. The water production after perihelion decreases much faster than its rise before perihelion.

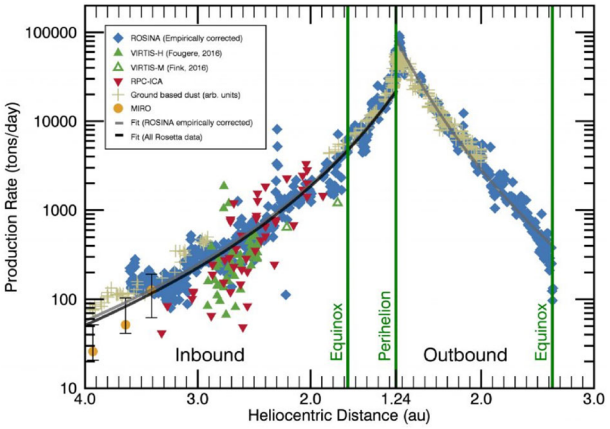

Fig. 24 The water production rate measured (between June 2014 and May 2016) at Comet 67P as a function of the comet's distance from the Sun. The measurements are from ROSINA-DFMS (blue diamonds); MIRO (yellow circles); VIRTIS-H (solid green triangles); VIRTIS-M (unfilled green triangles); RPC-ICA (red triangles). The dust production rate, estimated from ground-based observations, is indicated by tan crosses. Image adapted from Hansen et al. (2016)

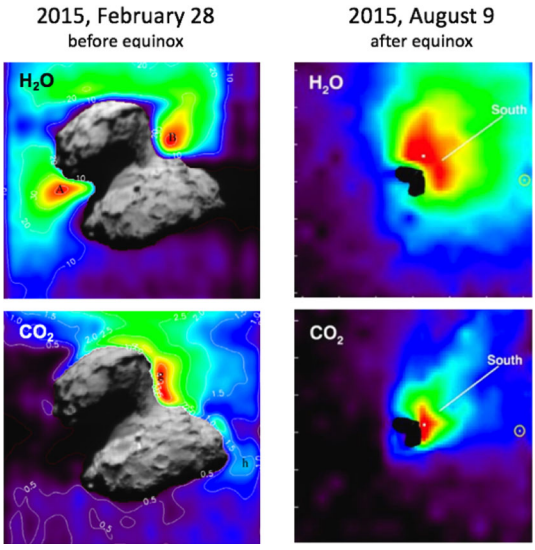

Fig. 25 Left: distribution of CO_2 and H_2O emission (2015 Feb 28) in the coma of 67P from VIRTIS-M (Fink et al. 2016). Right: VIRTIS-H raster maps of the H_2O 2.7 μm and CO_2 4.3 μm bands. H_2O and CO_2, on August 9, 2015. The projection of the rotation axis (southern direction) and the direction of the Sun are indicated (Bockelée-Morvan et al. 2016)

This evolution of the production rate with heliocentric distance suggests that, during the long and quite cold summer of northern hemi-nucleus, there is enough insolation to deplete the upper layers of supervolatiles, such as CO_2, but not H_2O which remain the dominant species in the northern hemisphere. The short, but warmer summer in the southern hemisphere sublimates completely all the volatiles in the upper layers, exposing new materials always. In Fig. 25 two maps of the H_2O and CO_2 emission are reported before and after the inbound equinox, corresponding to the northern summer (February 28th, 2015) and the southern summer (August 9, 2015), respectively.

To better understand cometary activity and more specifically the presence of dust structures in cometary comae, Dalla Corte et al. (2016) mapped the spatial distribution of dust density in the coma tracking 67P's seasons. The dust particles detected by GIADA and OSIRIS (Rotundi et al. 2015) from the beginning of the mission belong to two families: (1) compact particles (size range from 0.03 to 1 mm, density $\sim$ 2 kg m^{-3}), containing materials processed within the solar nebula and (2) a more primitive component composed of fluffy aggregates (size range from 0.2 to 2.5 mm and equivalent bulk density $<$1 kg m^{-3}) of sub-micron grains, probably linked to interstellar dust (Fulle et al. 2015).

The largest chunks escaping the nucleus gravity, ranging from centimeter-sized pebbles at 3.5 AU inbound, to meter-sized chunks at perihelion emerging from localized areas on the comet surface have also been observed in several OSIRIS images (Rotundi et al. 2015; Agarwal et al. 2016; Fulle et al. 2016a).

MIDAS found particles consistent with hierarchical agglomerates showing compact packing (the majority) and some are highly porous and fractal. Both kind of particles are tens of micrometers in size and are composed of subunit size distributions with similar mean values of $1.48 + 0.13 - 0.59\,\mu$m for the porous particles and $1.36 + 0.15 - 0.59\,\mu$m for the compact ones. The fluffy fractal particles are interpreted as agglomerates in the protoplanetary disc and preserved in the comet (Mannel et al. 2016; Fulle and Blumm 2017). The similarity of these subunits of both fractal and compact dust indicates a common origin dominated by slow agglomeration of equally sized aggregates. Dust particles and the observed larger aggregates (10 cm–1m) are lifted in the coma by the ubiquitous outgassing from all the surface and by the stronger action of localized outburst (Vincent et al. 2016a; Grün et al. 2016). Many outbursts were detected (Fig. 26) in the OSIRIS NAC and the navigation camera images, having

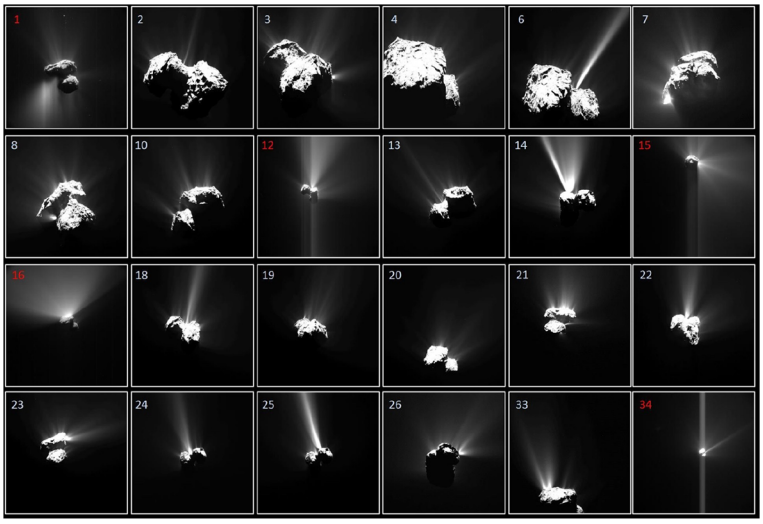

Fig. 26 Mosaic of the brightest OSIRIS NAC (white) and NavCam (red) outbursts detected by Rosetta from 2015 July to September (Vincent et al. 2016a, b) (ESA/Rosetta/MPS for OSIRIS Team MPS/UPD/LAM/IAA/SSO/INTA/UPM/DASP/IDA)

three main dust plume morphologies: a narrow jet, a broad fan and a combination of both of the previous. The outburst sources are mainly located at the boundaries of different morphological regions, especially where steep scarps or cliffs are present. Outbursts occur either at local dawn, possibly triggered by thermal stresses linked to the rapid change of temperature, or in early afternoon, probably related to a diurnal or seasonal heat wave reaching local volatiles reservoirs buried under the first surface layer. Vincent et al. (2016b) observed that most outbursts are located near collapsed cliffs presenting evidence of mass wasting and suggested that most of the dust is generated during the cliff collapse and lifted away by the surface gas flow without explosions, owing to the absence of cohesion forces linking the grains to the nucleus surface. The measured accelerations of the dust particles and aggregates are up to a factor 10 larger than gravity. The temporal brightness decreases in at least 1/3 of the aggregates, possibly indicating the ongoing sublimation of embedded ice. Large particles rapidly decouple from the gas after ejection from the surface: particles ejected at speeds of < 0.5 m s^{-1} fail to escape in the coma and fall back to the surface. On the other hand, particles faster than about 1.0 m s^{-1} either escape or collide with some surface obstacle on their way, falling back on the surface. The dust particles/aggregates are ejected at speeds in the intermediate range or escape or are re-distributed over the entire nucleus, generating the observed airfalls (Thomas et al. 2015a) and contributing to the activity. The re-impacting particles have the potential to be gas sources with the release of the embedded ice and can lead to gas emission on a global scale.

67P nucleus has a dust-to-water mass ratio (dust mass loss rates/water vapor mass loss rate) of 6 from 3.6 AU to perihelion (Rotundi et al. 2015; Fulle et al. 2016a), which becomes a dust-to-gas ratio of 4–5, taking into account the abundance of minor species (Hassig et al. 2015) and the dust bulk densities. At perihelion and just after, the dust-to-water mass ratio ranges from 6 to 100 (Fulle et al. 2016a). Based on the water production rate, Hansen et al. (2016) provide an estimation of the comet water loss to space of some 6.4 billion (10^9) kg over the period monitored by Rosetta (2014 June–2016 May), with the most intense mass loss near perihelion. The total mass loss, taking into account the amount of dust loss and other gas molecules (in particular, CO_2, CO and O_2), could be roughly ten times larger than that, so $\Delta M/M = (6.411 \pm 2) \times 10^{-3}$, and, if distributed uniformly across the comet nucleus, it would translate into a reduction of 2–4 m per orbit. In the hypothesis that the orbit of the comet does not undergo major changes and the nucleus mass loss could be considered constant, and that the comet nucleus does not break dawn (Hirabayashi et al. 2016), 67P/Churyumov–Gerasimenko would survive in the next millennium.

The activity is strictly connected with the magnetic/plasma environment of the comet. Measurements taken during Philae's descent and landing by its ROMAP and RPC-MAG instrument indicate that the nucleus of 67P has no magnetic field of its own (Auster et al. 2015). These instruments determined also the characteristics of the low-frequency plasma waves, which propagate predominantly from the nucleus toward the Sun with a mean phase velocity of ~ 5.3 km s^{-1}, a wavelength of $\sim$ 660 km and an average frequency of ~ 8 mHz (Heinisch et al. 2017). At heliocentric distance of 3.4 AU two regions characterized the early plasma atmosphere of the comet: an outer region dominated by the solar wind's convection electric field and a high-plasma density (HDR) region, at about 30 km from the nucleus for the northern

latitudes (Yang et al. 2016). The main cometary plasma sources identified are H_2O photoionization by solar extreme ultraviolet (EUV) radiation and energetic electron-impact ionization (Galand et al. 2016). A dense and warm population of electrons ($\sim 10\ cm^{-3}$ and ~ 16 eV) and a second rarefied and hot population ($\sim 0.01\ cm^{-3}$ and ~ 43 eV) were described by Broiles et al. (2016). The former is composed of two sub-populations: one with T <8.6 eV (unaffected by neutral density and weakly correlated with magnetic field strength) and an other with T >8.6 eV (correlated with neutral density and heated by lower hybrid waves). When the plasma is dominated by water ions from the comet, a situation with magnetized electrons and unmagnetized ions is favorable for the generation of lower hybrid waves. These waves can transfer energy between ions and electrons and reshape the plasma environment of the comet (André et al. 2017). Indeed, there is a need for a process to accelerate electrons to energies > 40–50 eV, to produce H atoms emitting Lyman-beta photons detected by ALICE, since photo-electrons produced from ionization of H_2O are not energetic enough (as well as solar wind electrons with ~ 5 eV).

Interaction of the solar wind with the comet is highly turbulent and stronger than expected for this weakly outgassing comet (Clark et al. 2015) and can be at the origin of the presence in the coma of refractory elements Na, K, Si, and Ca, presumably sputtered from grains residing on the surface (Wurz et al. 2015). The interaction between a comet and the impinging solar wind modifies the magnetic field in the environment of a comet and a comet magnetosphere emerges, which excites instability-driven waves and turbulence in the surrounding plasma. The plasma flow is strongly deflected from the Sun–comet direction (Koenders et al. 2016). The solar wind experiences large deflections (up to > 45°) in the weak coma. The average ion velocity slows from the mass loading of newborn cometary ions, which also slows the interplanetary magnetic field relative to the solar wind ions and subsequently creates a Lorentz force in the frame of the solar wind (Broiles et al. 2015). The flux of accelerated water ions moving from the upstream direction back toward the nucleus is a strongly nonlinear function of heliocentric distance and reach a flux similar to that of the solar wind at a Sun distance of 2.0 AU (Nilsson et al. 2015).

In the period April 2015–February 2016, there was a diamagnetic cavity around the comet, which had a highly variable outer boundary (Nemeth et al. 2016) whose properties depended on the long-term trend of the outgassing rate, but did not respond to transient events at the spacecraft location, such as outbursts or high neutral densities (Goetz et al. 2016).

5.4 Composition

The surface composition of 67P is one of the most puzzling questions. The imaging spectrometer VIRTIS instrument mapped the complete surface of the comet on the visible and near infrared from 250 to 5000 nm, showing a body covered by dark dehydrated refractory materials. The first VIRTIS results (Capaccioni et al. 2015) show the three major regions (head, body and neck) with very similar general behavior with reddish spectra (at different slopes), low albedo and a strong absorption in the range 2900–3600 nm associated with organics (Fig. 27). The thermal emission measured between 3500 and 5000 nm allowed to measure the surface temperature between

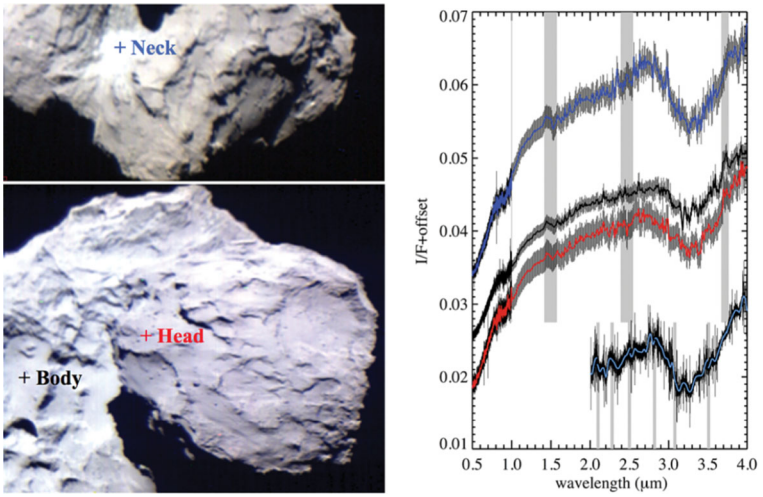

Fig. 27 Images acquired by VIRTIS-M and relative spectra (0.5–4.0 μm) corresponding to the different color (red, black, and blue curves) of the three different region (on the left). The fourth spectra (right, last on the bottom) has been obtained by VIRTIS-H in the 2–4 μm range (from Capaccioni et al. 2015)

180 and 230 K during daytime. The organic-rich surface is compatible with opaque minerals associated with non-volatile organic macromolecular material with a complex mixture of carbon–hydrogen and/or oxygen–hydrogen groups.

The capability of OSIRIS with the photometry in 20 filters (in the range 250–1000 nm) allowed to study the surface of the comet with spectrophotometry at higher resolution. The obtained results by Fornasier et al. (2015) show also a red spectral behavior with no specific bands, except the potential absorption at 290 nm, possibly due to SO_2 ice. The surface reflectance has been divided in three groups associated with different compositions corresponding to low spectral slope (bluer regions), average spectral slope and high spectral slope (reddest regions). Perna et al. (2017) using the same data, and a multivariate statistical technique obtained the same results and found a fourth group (with an increase of the flux at 700–750 nm) connected to the cometary activity. De Sanctis et al. (2015) was the first to detect water ice on the surface of the neck of the comet 67P with VIRTIS observations. They detected a shift of the band from 3200 to 3000 nm. The water ice appeared and disappeared in a cyclic pattern following local illumination. They suggested a diurnal cycle of water ice of sublimation and condensation of ice, varying with the illumination which could contribute to different erosions of the surface, producing different morphologies. Filacchione et al. (2016a, b) reported the identification of water ice on two debris falls in the Imhotep region. The ice was exposed on the walls of elevated structures and on the base of the walls.

Barucci et al. (2016), combining the images at different lighting geometries obtained at high resolution by OSIRIS and the spectra by VIRTIS, confirmed the existence of a larger number of water ice spots. The largest bright spots with high albedo, observed by OSIRIS, were checked by spectroscopy and the clear features at 1.5 and 2 microns confirmed the evidence of water ice (see for example Fig. 28). The high-resolution

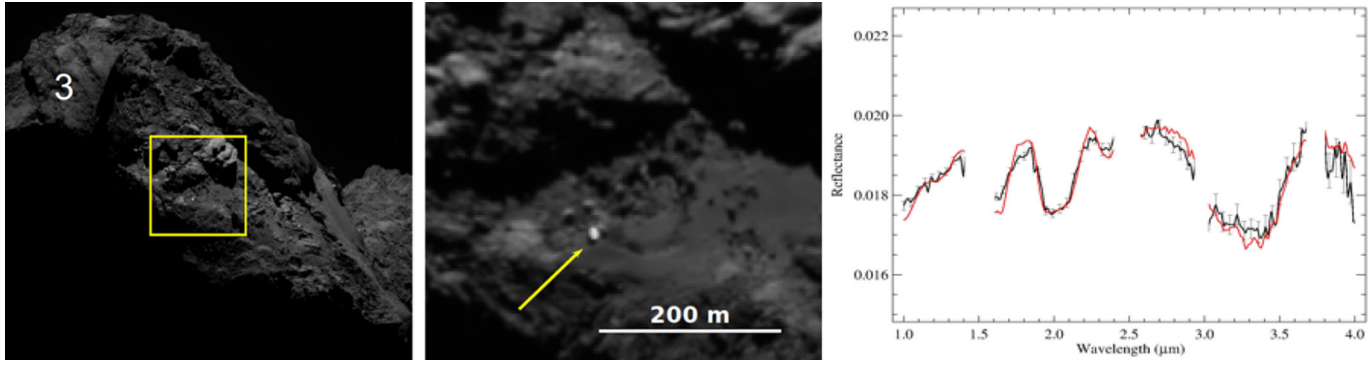

Fig. 28 Bright spot (about 11 m) is visible in the Khonsu region as observed by OSIRIS on April 2015. The ice spot appears like a bright boulder close to a pancake feature (apparently composed of three broad layers) at the center of the Khonsu region and disappears completely in May. The spectrum reported in black on the right has been taken by VIRTIS (Barucci et al. 2016). In red is the model computed as best fit with few % of H_2O ice and the average dark material on the surface. The gaps in the spectral ranges correspond to order-sorting filter-junction wavelengths that could produce unreliable features

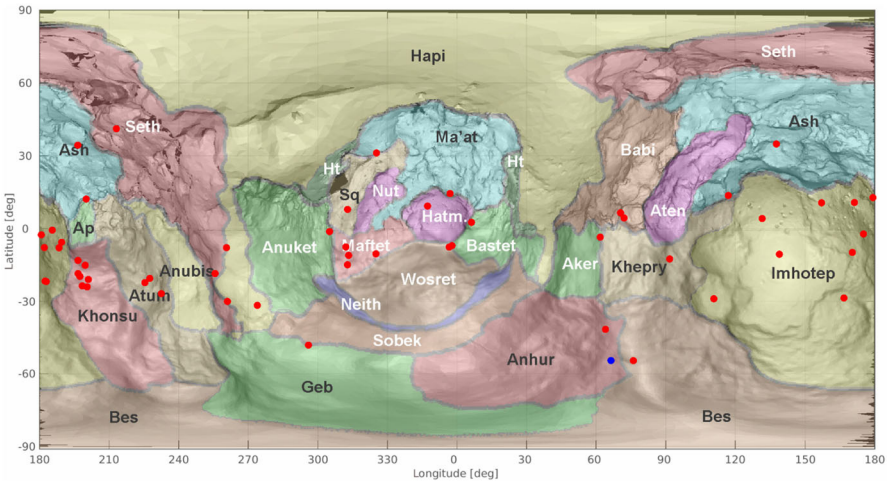

Fig. 29 Map of 67P in a cylindrical projection with all 26 defined region reported in different colors. The red points represent the detected H_2O ice spots, while the blue point represents the CO_2 spot

images obtained by OSIRIS allowed to identify a large quantity of bright spots of different sizes. The ice spots are distributed on the two lobes in locations which remain in shadow for longer intervals (see map in Fig. 29). For each spot, the temperature changes because of the local diurnal variation of the solar input, seasonal effects, shadowing and/or self-heating. Some of the spots are stable for several months, while others show temporal changes connected to diurnal and seasonal variation. Water ice is present on the surface substrata where solar illumination plays an important role. Cometary activity, triggered below the surface, may influence the local surface properties. All the water spots have been found on consolidated dust-free materials, either on freshly exposed outcropping regions or in boulders with the majority concentrated in equatorial latitudes. A majority of these spots are located close to dust jets and outbursts observed in cometary summer (Vincent et al. 2016a, b) for which the majority originates also from rough terrains and fractured walls rather than smooth areas. One very large spot of 1500 m^2 rich in ice was observed in the Anhur region by Fornasier et al. (2016, 2017), which vanished in 10 days with evidence of frosts sublimating in a few minutes. A few weeks earlier, Filacchione et al. (2016a, b) detected the first and only presence of the CO_2on the surface of the comet at the same location. This exposed ice was observed for a short time after the comet exited from local winter and, successively following the increased illumination, the CO_2 ice disappeared within about 3 weeks. Though CO_2 is one of the most abundant species in the cometary nuclei, it is rarely observed on the surface. Seasonal and diurnal color variations were also reported, as well as frosts sublimating in few minutes (Fornasier et al. 2016).

Understanding the composition of the surface of the comets remains a puzzling problem, though laboratory simulations (Quirico et al. 2016) are ongoing, to try to better interpret the possible composition with study on cometary grains and on interstellar ice analogs.

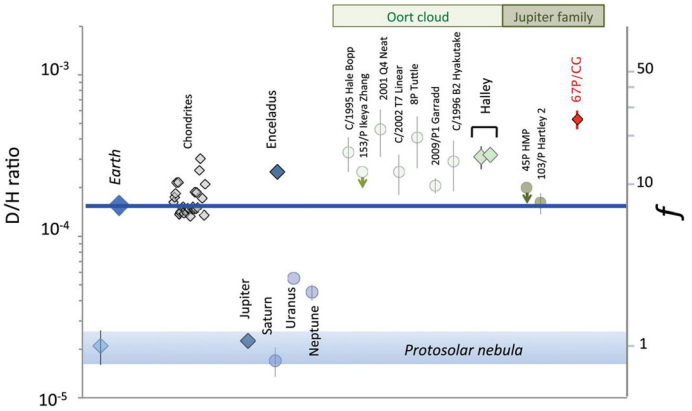

Fig. 30 *D*/*H* in different objects of the solar system (from Altwegg et al. 2015)

The COSIMA mass spectrometer onboard the spacecraft detected more than 27,000 particles in the vicinity of comet 67P/Churyumov–Gerasimenko. Fray et al. (2016) with deep chemical analysis of two of these particles, named Kenneth and Juliette, revealed the presence of solid organic matter, in which the carbon is bound in very large macromolecular compounds, analogous to the insoluble organic matter found in the carbonaceous chondrite meteorites. The authors concluded that the observed cometary carbonaceous solid matter could have the same origin as the meteoritic insoluble organic matter, but had suffered less modifications before and/or after incorporation into the comet.

One of the most appealing results obtained by Rosetta has been obtained using ROSINA mass spectrometer, which was designed to measure isotopic ratio. Altwegg et al. (2015) reported the *D*/*H* of the comet 67P to be $5.3 \pm 0.7 \times 10^{-4}$ which corresponds to about three times the terrestrial value. As shown in Fig. 30, this value is not at all consistent with the values of JFC (Jupiter Family Comets) already published and implies a hetereogeneity on the JFC and a possible diverse origin. The result is a fundamental contribution on the discussion of the provenance of water and organic on the Earth and the emergence of life which has been discussed for a long time. This makes it unlikely that water found on Earth came from comets such as 67P. Altwegg et al. concluded that this new result supported models advocating that primitive asteroids (composed of carbonaceous chondrites) could be the origin of the oceans on the Earth and the terrestrial atmosphere.

Thanks to ROSINA, a large number of molecules have been discovered in the comet atmosphere. Our present knowledge of the composition of the cometary nucleus is still based on investigation of the coma. Another important discovery is the detection of large amounts of free molecular oxygen (O_2) gas, surrounding the comet (Bieler et al. 2015b). The comets in our solar system are those left over from planetesimal swarms from which the planets formed, and the present models suggest that molecular oxygen should have disappeared by the time 67P was created (about 4.6 billion years ago). Molecular oxygen has never been detected before in cometary comas due to the difficulty to detect oxygen from ground-based observations. In situ measurements indicate

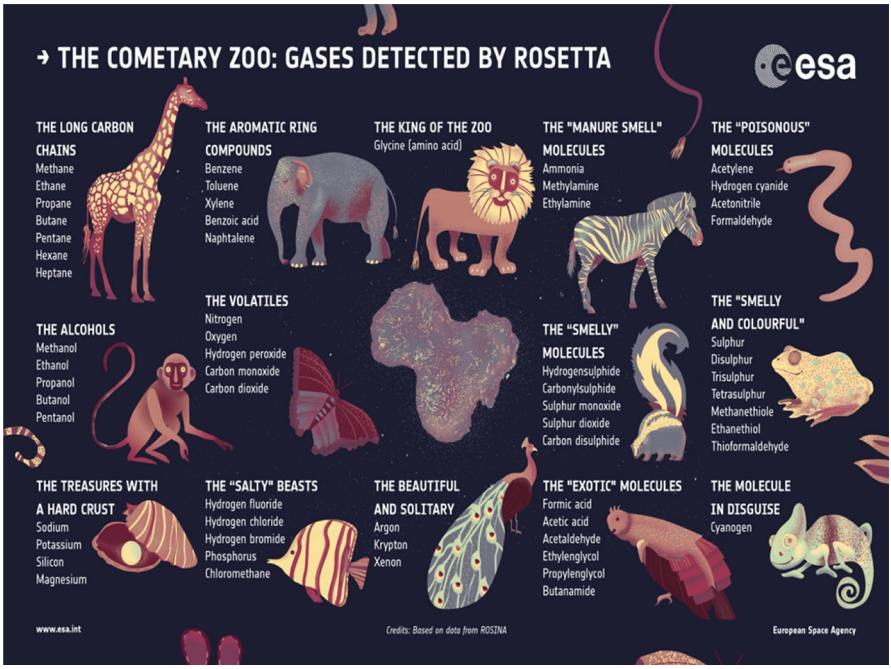

Fig. 31 The Cometary zoo: molecules detected by ROSINA instrument. Here they are creatively associated with different "animals". Credit by ESA and ROSINA team

that the O_2/H_2O ratio is isotropic in the coma and does not change systematically with heliocentric distance, suggesting that primordial O_2 was incorporated into the nucleus during the comet's formation. Rubin et al. (2015) report the direct ROSINA in situ measurement of N_2 and found the N_2/CO ratio at levels that are depleted compared to those in the primordial solar system. Depletion of such a magnitude suggests that cometary grains formed at low-temperature conditions below $\sim$ 30 K. CO and CO_2 are much more abundant compared to the abundances detected on the other JFCs. The abundances are different between summer and winter hemispheres. Uunderstanding the cometary activity was one of the main goals of the Rosetta mission. Bockelée-Morvan et al. (2015) using the VIRTIS-H (channel at high resolution) observed the activity of the comet and analyzed the first observations of H_2O and CO_2. Water production was observed mainly above the neck and it was weak from the region with low solar illumination, while CO_2 was outgassing from both illuminated and non-illuminated regions at the same rate, indicating that CO_2 sublimated at a depth that was below the diurnal skin depth.

Besides the main components of gases, ROSINA detected a wide variety of chemical species including ingredients that were crucial to the origin of life. A summary of species detected by ROSINA is reported in the cometary zoo schema (Fig. 31). Glycine, one amino acid important to life, is analogous to the lion as king of the zoo. Volatile species such as CO, CO_2, N and O are analogous to butterflies. Many carbon chains, such as methane and ethane, up to long chains like propane are by analogy like giraffes.

The many alcoholic compounds are comparable with monkeys. Some other species found including acetylene, hydrogen cyanide and formaldehyde could be poisonous and are associated with snakes. Some noble gases were also found: argon, xenon and krypton, which do not react easily with other molecules and are considered to be like the aloof peacock (beautiful and solitary), and so on for the other species; see Fig. 31.

Measurements by the COSAC and Ptolemy instruments on the Philae's lander revealed 16 organic compounds, 4 of which were seen for the first time on a comet, including acetamide, acetone, methyl isocyanate and propionaldehyde (see Sect. 3.3 for details).

6 The origin

Comets represent the most primitive materials of our solar system and are an invaluable repository of information on its early history. The knowledge of their nature and evolution could provide the key to understand the chemical, mineralogical and physical properties of the proto-solar nebula materials from which they formed. In particular, their internal structure, as well as their activity, may provide Rosetta Stone-like clues to the accretion processes forming these bodies.

The large amount of data collected by the Rosetta instruments on comet 67P/Churyumov–Gerasimenko provide insights to unveil the origin of this weird object. Observations of the comet 67P/Churyumov–Gerasimenko by Rosetta show a bi-lobed nucleus, extensively layered, with low bulk density, high dust-to-ice mass ratio (implying high porosity) and weak strength except for a thin sintered surface layer. The comet is rich in supervolatiles (CO, CO_2) and may contain amorphous water ice. The new molecules discovered in the atmosphere of comet 67P (Altwegg et al. 2016) and the presence of interstellar like complex organic compounds in its nucleus (Capaccioni et al. 2015; Quirico et al. 2016) show that comets are made of pristine material synthesized in the solar nebula or during the earlier stage of the solar system formation. The knowledge of molecules abundances and their diversity is important to understand the formation conditions of aggregates in the primitive solar nebula. Fulle et al. (2016b) suggest that the compact particles ejected by the comet are millimeter- to centimeter-sized pebbles, aggregates of ices and non-volatile materials with an internal macro porosity of 40%, that formed all planetesimals by gravitational accretion (Zsom et al. 2010; Wahlberg Jansson and Johansen 2014). Moreover, Fulle and Blumm (2017) show that the flux of fractal particles measured by Rosetta implies that the 67P nucleus grew by packing gently together centimeter-sized pebbles and fractal particles that filled the voids among pebbles. This structure cannot have survived catastrophic collision, which would have compacted and/or caused loss of most fractal particles: the fractals can be preserved in a cometesimal if they are formed through a gentle gravitational collapse (mutual collision speeds $<<1$ m s^{-1}) of a mixture of pebbles and fractals.

The average dust bulk densities of the 67P pebbles measured by Fulle et al. (2016b), coupled to the nucleus bulk density, provide the average dust-to-ice mass ratio $\delta = 8.5$ and is consistent with a composition of a mixture in average volume abundances of (15 ± 6) % of ices, (5 ± 2) % of Fe-sapheads, (28 ± 5) % of silicates and (52 ± 12) %

of hydrocarbons. This composition corresponds both to the solar and CI-chondritic chemical abundances. The pebbles with a microporosity of (52 ± 8) %, imply an average porosity for the 67P nucleus of (71 ± 8)%. Moreover, the dust-to-water ratio of 6 becomes a dust-to-gas ratio in the range 4–5 from outbound to the perihelion, considering also the abundances of minor species (Hassig et al. 2015): the elemental abundances of CI chondrites imply a dust-to-gas mass ratio of 3 and a porosity of at least 70 % (Davidsson et al. 2016). This suggests that 67P accreted in a region of the proto-solar nebula drier than those where CI chondrites have formed.

There is a general agreement in considering that comet 67P shape is derived from two objects that have formed a contact binary via a gentle merger. Jutzi and Asphaug (2015) simulated the impact of two cometesimals in two cases of interest: layer-forming splats and mergers resulting in bi-lobed shapes that could be a direct result of accretionary collisions. For bodies with low tensile strength, the simulation results can explain the morphology of cometary nuclei and their low bulk densities. Rickman et al. (2015) suggest that the two lobes formed in the same environment, owing to their similarity in composition. Estimation of the collisional rate in the primordial planetary disk shows that most comets of similar size to 67P are likely collisional fragments, although survival of primordial planetesimals cannot be excluded (Morbidelli and Rickman 2015). The reconstruction of the comet nucleus based on the orientation and distributions of the layers shows that the two lobes are the expression of two independent objects with layered envelopes, formed before they merged. Massironi et al. (2015) concluded that the structure of the comets provides evidence that gentle low-velocity collisions occurred between fully formed planetesimals. The layering structure rules out a rubble-pile structure up having multi-meter scale components, favoring a scheme where each lobe was the result of the accretion of smaller centimeter-scale (or smaller) pebbles enveloped, at an advanced stage of growth, within denser outer surface layers.

All these considerations are based on two hypotheses: that the 67P nucleus accreted by (1) a primordial collisional coagulation, producing "primordial" rubble piles or by (2) re-accretion of fragments after an energetic impact onto a larger parent body, which originated the collisional rubble piles. The latter process, because of the thermal processing due to ^{26}Al together with the heating by the compaction due to collisions, produce bodies in the size range of 50–200 km in diameter that are dense, compacted, strong, heavily depleted in supervolatiles and poor in amorphous water ice, and that have experienced extensive aqueous alteration. Irregular satellites of Saturn and Jupiter, as Phoebe and Himalia, respectively, could be examples of this population. These collisional rubble piles inherit all the properties of their parent bodies. In contrast, the former process produced rubble piles which are "primordial" in the sense that they preserve the properties of the pristine materials from which comet formation took place starting in the solar nebula and ending in primordial disk (Davidsson et al. 2016). the Streaming instabilities in a low-mass, dynamically cold, primordial disk form TNOs at sizes of about 50–400 km, few hundreds of them grow slowly to the size of triton, causing little viscous stirring during growth. Comets form by hierarchical agglomeration out of material left over by the TNOs formation. In such environment, medium-sized TNOs cannot break into collisional rubble piles, because of the low collision probability, allowing the primordial comets to survive the age of the solar

system. Radiometric dating of some of the stardust samples (Nakashima et al. 2015 and therein references) implies that the comet nuclei had a slowly increasing growth which allows them (1) to avoid thermal processing by short-lived radionuclides that would lead to loss of supervolatiles and (2) to incorporate 3 Myr-old material from the inner solar system. Porous single-lobe nuclei agglomerated in the solar nebula and continued to grow in a mildly viscously stirred primordial disk, where denser outer layers were formed. Bi-lobed comets accreted from mergers of cometesimals, born in the same disc region where the relative speeds were <1 ms^{-1}.

Owing to the observed properties of 67P, and those of the other flown-by short period comets, the comet nuclei seem to be primordial rubble piles, and not collisional rubble piles.

7 Insights learned on the primordial Solar System from the Rosetta mission

The observations and the analysis of the data collected for more than 2 years on the comet P67 from Rosetta provided a complete portrait of the nature of the comet today and allowed the instrument teams to investigate and to characterize the modifying processes which the comet has undergone during its journey around the Sun. Moreover, Rosetta observations shed light on the primeval processes concerning the formation of the solar system:

- The discovery in the coma of 67P of molecular hydrogen, nitrogen and of the unexpected high abundance of molecular oxygen (4% with respect to water) indicated that all were incorporated in the nucleus in a low-density and a low-temperature environment, as the pre-solar cloud. Moreover, the O_2 high reactivity suggests that it was formed in the ice envelopes of interstellar dust grains, which would have survived in the nucleus since its accretion.
- The *D*/*H* ratio in the comet water is three times that found of the Earth's oceans. In the Jupiter-family comets, this ratio shows a wide variation, suggesting a complex *D*/*H* distribution in the solar nebula or a possible existence of multiple reservoirs.
- The ice content in 67P matches that inferred in Kuiper belt objects, $20 \pm 12\%$ on average volume abundance, and suggests a water content in all trans-Neptunian objects lower than in CI chondrites. The value of the dust/gas ratio has been estimated to vary from 4 to 5 when 67P comes from 3.5 AU to perihelion, while the dust/gas mass ratio of CI chondrites is 3. This implies that the region of the proto-solar nebula where 67P accreted may have been drier than those where CI chondrites have formed.
- The compact particles, ejected by comet 67P and detected by GIADA, are believed to be millimeter- to centimeter-sized pebbles, aggregates of ices and non-volatile materials that solar system formation models predict to be the building blocks of planetesimals.
- Comet 67P has a bi-lobed shape; it has been formed by gentle, low-velocity collisions that occurred between two kilometer-sized planetesimals, as indicated by the distinct 'onion-like' stratifications which characterize the two lobes. In fact, the comet's "body" is enveloped by a continuous series of layers, which are indepen-

dent of an analogous stratified set on the "head". The structural similarities between the two lobes indicate the two planetesimals that formed 67P underwent a similar stratification process during their primordial accretion, though they formed independently, in the early stages of the solar system.

- The reflectance spectra collected across the comet surface are red and, in the visible and near-infrared region, show only a broad absorption band centered at 3.2 μm. The low albedo of 67P is accounted for by a dark refractory polyaromatic carbonaceous component mixed with opaque minerals. The nature of this component is difficult to be determined: water ice contributes to this feature only in the "neck" region; COOH in carboxylic acids along with the NH_4^+ is a highly plausible candidate. Spectral analogs of photolytic/thermal residues produced in laboratory from interstellar ice analogs could also indicate a pre-proto-solar nebula origin of these complex organics.

The above information would lead to a formation scenario for the comet 67P, which starts with interstellar ices and grains imbedded in a first generation of pebbles that accreted in a cold and extremely diffuse environment. In this early phase, the pebbles grew from refractory minerals, complex organic materials and water (with variable content of the deuterium) in regions of the proto solar nebula drier than those where the CI primitive meteorites formed. These pebbles slowly built kilometer-sized objects through a layering process which lent the structure of the growing planetesimals. An extremely low-velocity collision occurred between two of these planetesimals forming the bi-lobate nucleus of 67/P.

Many questions remain unanswered. Are the observed dust agglomerates primitive pebbles?

Does the nucleus contain components of interstellar matter? What is the age of surface material? What is the composition of the ubiquitous dark complex organics? How old are the subsurface materials? Do the layers have different ages? What is the nucleus' internal structure?

The answers to these fundamental questions require measurements with exceptionally high precision and sensitivity. Such measurements cannot be performed by a robotic spacecraft and therefore require a sample returned to terrestrial laboratories where instrumentation is unconstrained by mass, power, stability, etc. The most demanding measurements are those required to date the major events in the history of a sample and to investigate the organic components. Laboratory techniques determine the time interval between the end of nucleosynthesis and agglomeration, the duration of agglomeration, time of accumulation, crystallization age, the age of major heating and degassing events, the time of metamorphism, the time of aqueous alteration and the duration of exposure to cosmic radiation.

The sample returned from such a body will contain material representative of the main components from the parent body. The abundance and distribution of newly synthetised short-lived radionuclides present in these earliest materials will provide a record of the nucleosynthetic events preceding the formation of the solar nebula. Insight into the nature of the molecular cloud from which the solar system was born will be obtained from a more comprehensive understanding of pre-solar grain populations in the early solar system, including their journeys through the interstellar medium

(ISM). The combined pre-solar studies will provide a new picture of the astrophysical setting of the birth of the solar system and may permit identification of the stellar event that triggered the collapse of the parental molecular cloud of the solar system. A uniquely complete structural record of a primitive body, from the nanometer scale (from the samples) to the internal structure of the body (from lander and orbiter radar) will provide new insight into the earliest stages of aggregation, accretion and assembly. The pristine material will allow clear record of the earliest processes in the protostellar disk, including radial transport mechanisms to the outermost regions.

The Rosettta mission has thus been a spectacular success in translating the earliest processes of planetary formation into our current language of scientific understanding. Rosetta has not only opened a window to the past, but also places us on a threshold for advancing the future of planetary exploration. The next major step in understanding the nature of the comets requires a sample return mission.

Acknowledgements The authors acknowledge the funding of the French national space agency Centre National d'Etudes Spatiales. We are grateful to all the Rosetta instrument teams and ESA Operations teams. The ESA Technical Directorate is also gratefully acknowledged.

References

Agarwal J, A'Hearn MF, Vincent J-B et al (2016) Acceleration of individual decimetre-sized aggregates in the lower coma of comet 67P/Churyumov–Gerasimenko. MNRAS 462:S578–S588

Altwegg K, Balsiger H, Bar-Nun A et al (2015) 67P/Churyumov–Gerasimenko, a Jupiter family comet with a high *D*/*H* ratio. Science 347:a0440

Altwegg K, Balsiger H, Bar-Nun A et al (2016) Prebiotic chemicals amino acid and phosphorus in the coma of comet 67P/Churyumov–Gerasimenko. Sci Adv 2(5):e1600285

André M, Odelstad M, Graham DB et al (2017) Lower hybrid waves at comet 67P/Churyumov–Gerasimenko. MNRAS 469:S29–S38

Auger A-T, Groussin O, Jorda L et al (2015) Geomorphology of the Imhotep region on comet 67P/Churyumov–Gerasimenko from OSIRIS observations. A&A 583:A35

Auster H-U, Apathy I, Berghofer G et al (2007) ROMAP: Rosetta magnetometer and plasma monitor. Sp Sci Rev 128:221–240

Auster H-U, Apathy I, Berghofer G et al (2015) The nonmagnetic nucleus of comet 67P/Churyumov–Gerasimenko. Science 349:aaa5102

Balsiger H, Altwegg K, Bochsler P et al (2007) Rosina Rosetta orbiter spectrometer for ion and neutral analysis. Sp Sci Rev 128:745–801

Bar-Nun, A, Barucci, MA, Bussoletti, E et al (1993) ROSETTA Comet Rendez Vous Mission. ESA SCI(93)7, September 1993

Barucci MA, Fulchignoni M, Fornasier S et al (2005) Asteroid target selection for the new Rosetta mission baseline 21 Lutetia and 2867 Steins. A&A 430:313–317

Barucci MA, Belskaya IN, Fornasier S et al (2012) Overview of Lutetia's surface composition. Planet Sp Sci 66:23–30

Barucci MA, Filacchoni G, Fornasier S et al (2016) Detection of exposed H_2O ice on the nucleus of comet 67P/Churyumov- Gerasimenko. Astron Astrophys 595:A102

Besse S, Lamy P, Jorda P et al (2012) Identification and physical properties of craters on asteroid (2867) Steins. Icarus 221:1119–1129

Besse S, Kueers M, Barnouin OS et al (2014) Lutetia's lineaments. Planet Sp Sci 101:186–195

Bibring J-P, Lamy P, Langevin Y et al (2007) Civa. Sp Sci Rev 128:397–412

Bibring J-P, Langevin Y, Carter J et al (2015) 67P/Churyumov–Gerasimenko surface properties as derived from CIVA panoramic images. Science 349:aaa0671

Biele J, Ulamec S, Maibaum M et al (2015) The landing(s) of Philae and inferences about comet surface mechanical properties. Science 349:aaa9816

Bieler A, Altwegg K, Balsiger H et al (2015a) Comparison of 3D kinetic and hydrodynamic models to ROSINA-COPS measurements of the neutral coma of 67P/Churyumov–Gerasimenko. A&A 583:A7
Bieler A, Altwegg K, Balsiger H et al (2015b) Abundant molecular oxygen in the coma of comet 67P/Churyumov–Gerasimenko. Nature 526(7575):678–681
Biver N, Hofstadter M, Gulkis S et al (2015) Distribution of water around the nucleus of comet 67P/Churyumov–Gerasimenko at 34 AU from the Sun as seen by the MIRO instrument on Rosetta. A&A 583:A3
Bockelée-Morvan D, Debout V, Erard S et al (2015) First observations of H_2O and CO_2 vapor in comet 67P/Churyumov–Gerasimenko made by VIRTIS onboard Rosetta. A&A 583:A6
Bockelée-Morvan D, Crovisier J, Erard S et al (2016) Evolution of CO_2, CH_4, and OCS abundances relative to H_2O in the coma of comet 67P around perihelion from Rosetta/VIRTIS-H observations. MNRAS 462:S170–S183
Boesswetter A, Auster U, Richter I et al (2009) Rosetta swing-by at Mars—an analysis of the RPMAP measurements in comparison with results af a 3-D mulyi-ion hybrid simulation and MEX/ASPERA_3 data. Ann Geophys 27:2383–2398
Broiles TW, Burch JL, Clark G et al (2015) Rosetta observations of solar wind interaction with the comet 67P/Churyumov–Gerasimenko. A&A 583(A21):7
Broiles TW, Burch JL, Chae K et al (2016) Statistical analysis of suprathermal electron drivers at 67P/Churyumov–Gerasimenko. MNRAS 462:S312–S322
Budnik F, Morley T (2007) Rosetta navigation at its Mars swing-by. In: Procceedings of 20th international symposium on space flight dynamics, Annapolis
Burch JL, Goldstein R, Cravens TE et al (2007) RPC-IES: the ion and electron sensor of the Rosetta plasma consortium. Sp Sci Rev 128:697–712
Capaccioni F, Coradini A, Filacchioni G et al (2015) The organic-rich surface of comet 67P/Churyumov–Gerasimenko as seen by VIRTIS/Rosetta. Science 337:a0628
Carr C, Cupido E, Lee CGY et al (2007) RPC: the Rosetta plasma consortium. Sp Sci Rev 128:629–647
Cawley SWH (1987) ICE observation of comet Giacobini–Zinner. Philos Trans R Soc Lond A323:405–420
Clark G, Broiles TW, Burch JL et al (2015) Suprathermal electron environment of comet 67P/Churyumov–Gerasimenko: observations from the Rosetta Ion and electron sensor. A&A 583:A24 6
Colangeli L, Lopez-Moreno JJ, Palumbo P et al (2007) The grain impact analyser and dust accumulator (GIADA) experiment for the Rosetta mission: design, performances and first results. Sp Sci Rev 128:803–821
Coradini A, Capaccioni F, Drossart P et al (2007) Virtis: an imaging spectrometer for the Rosetta mission. Sp Sci Rev 128:529–559
Coradini A, Grassi D, Capaccioni F et al (2010) Martian atmosphere as observed by VIRTIS-M on Rosetta spacecraft. JGR 115:E04004
Coradini A, Capaccioni F, Erard S (2011) The surface composition and temperature of asteroid 21 Lutetia as observed by Rosetta/VIRTIS. Science 334:492–494
Dalla Corte V, Rotundi A, Fulle M et al (2016) 67P/C-G inner coma dust properties from 22 au inbound to 20 au outbound to the Sun. MNRAS 462:S210–S219
Davidsson BJR, Sierks H, Güttler C et al (2016) The primordial nucleus of comet 67P/Churyumov–Gerasimenko. A&A 592:A63 30
Deshaprya P, Barucci MA, Fornasier S et al (2016) Spectrophotometry of the Khonsu region on the comet 67P/Churyumov–Gerasimenko using OSIRIS instrument images. MNRAS 462:274
De Sanctis MC, Capaccioni F, Ciarniello M et al (2015) The diurnal cycle of water ice on comet 67P/Churyumov–Gerasimenko. Nature 525:500–503
El-Maarry MR, Thomas N, Giacomini L et al (2015) Regional surface morphology of comet 67P/Churyumov–Gerasimenko from Rosetta/OSIRIS images. A&A 583:A26
El-Maarry MR, Thomas N, Gracia-Berná A et al (2016) Regional surface morphology of comet 67P/Churyumov–Gerasimenko from Rosetta/OSIRIS images: the southern hemisphere. A&A 593:A110
El-Maarry MR, Groussin O, Thomas N et al (2017) Surface changes on comet 67P/Churyumov–Gerasimenko suggest a more active past. Science 355(6332):1392–1395
Ercoli-Finzi A, Bernelli Zazzera F, Dainese C (2007) SDT—how to sample a comet. Sp Sci Rev 128:281–299
Eriksson AI, Boström R, Gill R et al (2007) RPC-LAP: the Rosetta Langmuir probe instrument. Sp Sci Rev 128:729–744

Feldman PD, Steffl AJ, Parker JW et al (2011) Rosetta–Alice observations of exospheric hydrogen and oxygen on Mars. Icarus 214:394–399
Feldman PD, A'Hearn MF, Bertaux J-L et al (2015) Measurements of the near-nucleus coma of comet 67P/Churyumov–Gerasimenko with the Alice far-ultraviolet spectrograph on Rosetta. A&A 583:A8
Filacchione G, de Sanctis MC, Capaccioni F et al (2016a) Exposed water ice on the nucleus of comet 67P/Churyumov–Gerasimenko. Nature 529:368–372
Filacchione G, Raponi A, Capaccioni F et al (2016b) Seasonal exposure of carbon dioxide ice on the nucleus of comet 67P/Churyumov–Gerasimenko. Science 354:1563–1566
Fink U, Doose L, Rinaldi G et al (2016) Investigation into the disparate origin of CO_2 and H_2O outgassing for Comet 67/P. Icarus 277:78–97
Fornasier S, Hasselmann PH, Barucci MA et al (2015) Spectrophotometric properties of the nucleus of comet 67P/Churyumov–Gerasimenko from the OSIRIS instrument onboard the ROSETTA spacecraft. A&A 583:A30
Fornasier S, Mottola S, Keller HU et al (2016) Rosetta's comet 67P sheds its dusty mantle to reveal its icy nature. Science 345:1566–1570
Fornasier S, Feller C, Lee J-C et al (2017) The highly active Anhur-Bes regions in the 67P Churyumov–Gerasimenko comet: results from OSIRIS/ROSETTA observations. MNRAS 469:S93–S107
Fougere N, Altwegg K, Berthelier J-J et al (2016) Direct simulation Monte Carlo modelling of the major species in the coma of comet 67P/Churyumov–Gerasimenko. MNRAS 462:S156–S163
Fray N, Bardyn A, Cottin H et al (2016) High-molecular-weight organic matter in the particles of comet 67P/Churyumov–Gerasimenko. Nature 538:72–74
Fulle M, Della Corte V, Rotondi A et al (2015) Density and charge of pristine fluffy particles from comet 67P/Churyumov–Gerasimenko. Astrophys J Lett 802:L2 5
Fulle M, Altobelli A, Buratti B et al (2016a) Unexpected and significant findings in comet 67P/Churyumov–Gerasimenko: an interdisciplinary view. MNRAS 462:S2–S8
Fulle M, Della Corte V, Rotondi A et al (2016b) Comet 67P/Churyumov–Gerasimenko preserved the pebbles that formed planetesimals. MNRAS 462:S132–S137
Fulle M, Blumm J (2017) Fractal dust constrains the collisional history of comets. MNRAS 469:S39–S44
Galand M, Héritier KL, Odelstad E et al (2016) Ionospheric plasma of comet 67P probed by *Rosetta* at 3 au from the Sun. MNRAS 462:S331–S351
Glassmeier K-H, Richter I, Diedrich A et al (2007) RPC-MAG: the fluxgate magnetometer in the ROSETTA plasma consortium. Sp Sci Rev 128:649–670
Goesmann F, Rosenbauer H, Roll R et al (2007) Cosac, The cometary sampling and composition experiment on Philae. Sp Sci Rev 128:257–280
Goesmann F, Rosenbauer H, Bredehöft JH et al (2015) Organic compounds on comet 67P/Churyumov–Gerasimenko revealed by COSAC mass spectrometry. Science 349:aab0689
Goetz C, Koenders C, Hansen KC et al (2016) Structure and evolution of the diamagnetic cavity at comet 67P/Churyumov–Gerasimenko. MNRAS 462:S459–S467
Groussin O, Sierks H, Barbieri C et al (2015) Temporal morphological changes in the Imhotep region of comet 67P/Churyumov–Gerasimenko. A&A 583:36
Gulkis S, Frerking M, Crovisier J et al (2007) MIRO: microwave instrument for Rosetta orbiter. Sp Sci Rev 128:561–597
Gulkis S, Allen M, von Allmen P et al (2015) Subsurface properties and early activity of comet 67P/Churyumov–Gerasimenko. Science 347:aaa0709
Grün E, Agarwal J, Altobelli N et al (2016) The 2016 Feb 19 outburst of comet 67P/CG: an ESA Rosetta multi-instrument study. MNRAS 462:S220–S234
Hansen KC, Altwegg K, Berthelier J-J et al (2016) Evolution of water production of 67P/Churyumov–Gerasimenko: an empirical model and a multi-instrument study. MNRAS 462:S491–S506
Hassig M, Altwegg K, Balsiger H et al (2015) Time variability and heterogeneity in the coma of 67P/Churyumov–Gerasimenko. Science 347:aaa0276
Heinisch P, Auster HU, Richter I et al (2017) Joint two-point observations of LF-waves at 67P/Churyumov–Gerasimenko. MNRAS 469:S68–S72
Hirabayashi M, Scheeres DJ, Chesley RS et al (2016) Fission and reconfiguration bilobate comets as revealed by 67P/Churyumov–Gerasimenko. Nature 534:352–355
Jorda L, Gaskell RW, Capanna C et al (2016) The global shape, density and rotation of comet 67P/Churyumov-Gerasimenko from pre-perihelion Rosetta/OSIRIS observations. Icarus 277:257–278

Jutzi M, Michel P, Benz W (2010) A large crater as a probe of the internal structure of the E-type asteroid Steins. A&A 509:L2–L5
Jutzi M, Asphaug E (2015) The shape and structure of cometary nuclei as a result of low-velocity accretion. Science 348(6241):1355–1358
Keller HU, Barbieri C, Lamy P et al (2007) OSIRIS: the scientific camera system onboard Rosetta. Sp Sci Rev 128:433–506
Keller HU, Barbieri C, Koschny D et al (2010) E-type asteroid (2867) steins as imaged by OSIRIS on board Rosetta. Science 327:190
Kissel J, Altwegg K, Clark BC et al (2007) Cosima high resolution time-of-flight secondary ion mass spectrometer for the analysis of cometary dust particles onboard Rosetta. Sp Sci Rev 128:823–867
Klingelhöfer G, Brückner J, D'Uston C et al (2007) The Rosetta alpha particle X-ray spectrometer (APXS). Sp Sci Rev 128:383–396
Koenders C, Goetz C, Richter I et al (2016) Magnetic field pile-up and draping at intermediately active comets: results from comet 67P/Churyumov–Gerasimenko at 20 AU. MNRAS 462:S235–S241
Kofman W, Herique A, Goutail J-P et al (2007) The comet nucleus sounding experiment by radiowave transmission (CONSERT): a short description of the instrument and of the commissioning stages. Sp Sci Rev 128:413–432
Kofman W, Herique A, Barbin Y et al (2015) Properties of the 67P/Churyumov–Gerasimenko interior revealed by CONSERT radar. Science 349:aaa0639
Küers M, Moissl R, Vincent J-B et al (2012) Boulders on Lutetia. Planet Sp Sci 66:71–78
Lee S, von Allmen P, Allen M et al (2015) Spatial and diurnal variation of water outgassing on comet 67P/Churyumov–Gerasimenko observed from Rosetta/MIRO in August 2014. A&A 583:A5
Le Roy L, Altwegg K, Balsiger H et al (2015) Inventory of the volatiles on comet 67P/Churyumov–Gerasimenko from Rosetta/ROSINA. A&A 583:A1
Lethuillier A, Le Gall A, Hamelin M et al (2016) Electrical properties and porosity of the first meter of the nucleus of 67P/Churyumov–Gerasimenko as constrained by the permittivity probe SESAME-/Philae/Rosetta. A&A 591(idA32):17
Leyrat C, Fornasier S, Barucci MA et al (2010) Search for Steins' surface inhomogeneities from OSIRIS Rosetta images. Planet Sp Sci 58:1097–1106
Luspay-Kuti A, Hässig M, Fuselier SA et al (2015) Composition-dependent outgassing of comet 67P/Churyumov–Gerasimenko from ROSINA/DFMS implications for nucleus heterogeneity? A&A 583:A4
Mall U, Altwegg K, Balsiger H et al (2016) High-time resolution in-situ investigation of major cometary volatiles around 67P/C-G at 31–23 AU measured with ROSINA-RTOF. Astrophys J 819:126 9
Mannel T, Bentley MS, Schmied R et al (2016) Fractal cometary dust—a window into early solar system. MNRAS 462:S304–S311
Marchi S, Massironi M, Vincent JB et al (2012) The cratering history of asteroid (21) Lutetia. Planet Sp Sci 66:87–95
Marchi S, Chapman CR, Barnouin OS et al (2015) Cratering on asteroids. In: Michel P et al (eds) Asteroid IV. Univ of Arizona Press, Arizona, pp 725–744
Massironi M, Simioni E, Marzari F et al (2015) Two independent and primitive envelopes of the bilobate nucleus of comet. 67P Nat 526:402–405
Morbidelli A, Rickman H (2015) Comets as collisional fragments of a primordial planetesimals disk. A&A 583:43 9
Morley T, Budnik F (2006) Rosetta Navigation at its first Earth Swing-by. In: Proocedings of the 19th international symposium on space flight dynamics, Kanazawa, Japan
Morley T, Budnik F (2009) Rosetta navigation for the fly-by of asteroid 2867 steins. In: Proceedings of the 21st international symposium on space flight dynamics, Toulouse
Morley T, Budnik F, Croon M et al (2012) Rosetta navigation for the fly-by of asteroid (21) Lutetia. In: Proceedings of the 25th international symposium on space flight dynamics, Pasadena
Mottola S, Arnold G, Grothues H-G (2007) The Rolis experiment on the Rosetta lander. Sp Sci Rev 128:241–255
Mottola S, Arnold G, Grothues H-G et al (2015) The structure of the regolith on 67P/Churyumov–Gerasimenko from ROLIS descent imaging. Science 349:aaa0232
Nakashima D, Ushikubo T, Kita NT et al (2015) Late formation of a comet Wild 2 crystalline silicate particle, Pyxie, inferred from Al-Mg chronology of plagioclase. Earth Planet Sci Lett 410:54–61

Newburn, RL Jr (1986) Halley Armada report. In: Prooceedings of the nineteenth annual electronics and aerospace systems conference, Washington, DC, Sept 8–10, 1986 (A87-40351 17-12) New York, Institute of Electrical and Electronics Engineers, Inc, 1986, p 165–173
Nemeth Z, Burch J, Goetz C et al (2016) Charged particle signatures of the diamagnetic cavity of comet 67P/Churyumov–Gerasimenko. MNRAS 462(Sul–1):S415–S421
Nilsson H, Lundin R, Lundin K et al (2007) RPC-ICA: the ion composition analyzer of the Rosetta plasma consortium. Sp Sci Rev 128:671–695
Nilsson H, Stenberg Wieser G, Behar E et al (2015) Evolution of the ion environment of comet 67P/Churyumov–Gerasimenko observations between 3.6 and 2.0 AU. A&A 583, A20, 8
Pajola M, Lazzarin M, Bertini D et al (2012a) Spectrophotometric investigation of Phobos with the Rosetta OSIRIS-NAC camera and implicaions for its collisional capture. MNRAS 427:3230–3243
Pajola M, Magrin S, Lazzarin M et al (2012b) Rosetta-Mars fly-by, February 25, 2007. Mem SAIt Suppl 20:105–113
Pajola M, Lazzarin M, Bertini I et al (2014) New hints on Phobos collisional capture origin from Rosetta-OSIRIS observation. Mem SAIt Suppl 26:75–80
Pajola M, Vincent J-B, Güttler C et al (2015) Size-frequency distribution of boulders $\geq$7 m on comet 67P/Churyumov–Gerasimenko. A&A 583:A37
Pajola M, Oklay N, La Forgia F et al (2016a) Aswan site on comet 67P/Churyumov–Gerasimenko: morphology, boulder evolution and spectrophotometry. A&A 592:A69 17
Pajola M, Lucchetti A, Vincent J-B et al (2016b) The southern hemisphere of 67P/ Churyumov–Gerasimenko: analysis of the preperihelion size/frequency distribution of boulders > 7m. A&A 592:L2 5
Pajola M, Hofner S, Vincent JB et al (2017) The pristine interior of comet 67P revealed by the combined Aswan outburst and cliff collapse. Nat Astron 1:0092
Pätzold M, Häusler B, Aksnes K et al (2007) Rosetta radio science investigations (RSI). Sp Sci Rev 128:599–627
Pätzold M, Andert TP, Asmar SW et al (2011) Asteroid 21 Lutetia: low mass, high density. Science 334:491–492
Patzold M, Andert T, Hahn M et al (2016) A homogeneous nucleus for comet 67P/Churyumov–Gerasimenko from its gravity field. Nature 530(7588):63–65
Perna D, Fulchignoni M, Barucci MA et al (2017) Multivariate statistical analysis of OSIRIS/Rosetta spectrophotometric data of comet 67P/ Churyumov–Gerasimenko. A&A 600:A115 9
Pommerol A, Thomas N, El-Maarry MR et al (2015) OSIRIS observations of meter-sized exposures of H20 ice at the surface of 67/Churyumov–Gerasimenko and interpretation using laboratory experiments. A&A 583:A25 16
Poulet F, Lucchetti A, Bibring J-P et al (2016) Origin of the local structures at the Philae landing site and possible implications on the formation and evolution of 67P/Churyumov–Gerasimenko. MNRAS 462(Supplement 1):S23–S32
Quirico E, Moroz LV, Schmitt B et al (2016) Refractory and semi-volatile organics at the surface of comet 67P/Churyumov–Gerasimenko: insights from the VIRTIS/Rosetta imaging spectrometer. Icarus 272:32–47
Rickman H, Marchi S, A'Hearn MF et al (2015) Comet 67P/Churyumov–Gerasimenko: constraints on its origin from Osiris observations. A&A 583:A44 8
Riedler W, Torkar K, Jeszenszky H et al (2007) MIDAS: the micro-imaging dust analysis system for the Rosetta mission. Sp Sci Rev 128:869–904
Rivkin AS, Clark BE, Ockert-Bell M et al (2011) Observations of 21 Lutetia in the 2–4 micron region with the NASA IRTF. Icarus 216:62–68
Rotundi A, Sierks H, Della Corte V et al (2015) Dust measurements in the coma of comet 67/P Churiumov–Gerasimenko inbound to the Sun. Science 347(6220):aaa3905 1–6
Rubin M, Altwegg K, Balsiger H et al (2015) Moleular nitrogen in comet 67P/Churyumov–Gerasimenko indicates a low formation temperature. Science 348:232–235
Schröder S, Mottola G, Arnold H-G et al (2017) Close-up images of the final Philae landing site on comet 67P/Churyumov–Gerasimenko acquired by the ROLIS camera. Icarus 285:263–274
Seidensticker KJ, Möhlmann D, Apathy I et al (2007) Sesame—an experiment of the Rosetta Lander Philae: objectives and general design. Sp Sci Rev 128:301–337
Sierks H, Lamy PL, Barbieri C (2011) Images of asteroid 21 Lutetia: a remnant planetesimal from the early solar system. Science 334:487–490

Sierks H, Barbieri C, Lamy PL et al (2015) On the nucleus structure and activity of comet 67P/Churyumov–Gerasimenko. Science 347:1044
Spohn T, Seiferlin K, Hagermann A et al (2007) Mupus a thermal and mechanical properties probe for the Rosetta Lander Philae. Sp Sci Rev 128:339–362
Spohn T, Knollenberg J, Ball AJ et al (2015) Thermal and mechanical properties of the near-surface layers of comet 67P/Churyumov–Gerasimenko. Science 349:aaa0464
Stern SA, Slater DC, Scherrer J et al (2007) Alice: the Rosetta ultraviolet imaging spectrograph. Sp Sci Rev 128:507–527
Stern SA, Parker JW, Feldman PD et al (2011) Ultraviolet discoveries at asteroid (21) Lutetia by Rosetta Alice ultraviolet spectrometer. Astron J 141:199–202
Thomas N, Barbieri C, Keller HU et al (2012) The geomorphology of (21) Lutetia: results from the OSIRIS imaging system on board ESA's Rosetta spacecraft. Planet Sp Sci 66:96–124
Thomas N, Davidsson BJR, El-Maarry MR et al (2015a) Redistribution of particles across the nucleus of comet 67P/Churyumov–Gerasimenko. A&A 583:A17
Thomas N, Sierks H, Barbieri C et al (2015b) The morphological diversity of comet 67P/Churyumov–Gerasimenko. Science 347:a0440
Trotignon JG, Lagoutte D, Michau JL et al (2005) Thermal plasma measurements in the earth plasmasphere by the mutual impedance probe onboard the Rosetta spacecraft. AGU fall meeting 2006, abstract #SM11B-0307
Trotignon JG, Lagoutte D, Michau JL et al (2006) Plasma Density and Magnetic Strength Measured in the Earth Plasmasphere by the Mutual Impedance Probe Onboard the Rosetta. Spacecraft AGU fall meeting 2006, abstract #SM11B-0307
Trotignon JG, Michau JL, Lagoutte D et al (2007) RPC-MIP: the mutual impedance probe of the Rosetta plasma consortium. Sp Sci Rev 128:713–728
Veverka J, Belton M, Klaasen K et al (1994) Galileo's encounter with 951 Gaspra: overview. Icarus 107:2–17
Vincent J-B, Bodewits D, Besse S et al (2015) Large heterogeneities in comet 67P as revealed by active pits from sinkhole collapse. Nature 523:63
Vincent J-B, A'Hearn MB, Lin Z-Y et al (2016a) Summer fireworks on comet 67P. MNRAS 462:S184–S194
Vincent J-B, Oklay N, Pajol M et al (2016b) Are fractured cliffs the source of cometary dust jets? Insights from OSIRIS/Rosetta at 67P/Churyumov–Gerasimenko. A&A 587:A14 15
Wahlberg Jansson K, Johansen A (2014) Formation of pebble-pile planetesimals. A&A 570:A47 10
Weiss BP, Elkins-Tanton LT, Barucci MA et al (2012) Possible evidence for partial differentiation of asteroid Lutetia from Rosetta. Planet Sp Sci 66:137–146
Wright IP, Pillinger CT (1998) Modulus-an experiment to measure precise stable isotope ratios on cometary materials. Adv Sp Res
Wright IP, Barber SJ, Morgan GH et al (2007) Ptolemy an instrument to measure stable isotopic ratios of key volatiles on a cometary nucleus. Sp Sci Rev 128:363–381
Wright IP, Sherida S, Barber SJ et al (2015) CHO-bearing organic compounds ar the surface of 67P/Churyumov–Gerasimenko revealed by Ptolemy. Science 349:aab0673
Wurz P, Rubin M, Altwegg K et al (2015) Solar wind sputtering of dust on the surface of 67P/Churyumov–Gerasimenko. A&A 583:A22 9
Yang L, Paulsson J, Simon Wedlund C et al (2016) Observations of high-plasma density region in the inner coma of 67P/Churyumov–Gerasimenko during early activity. MNRAS 462:S33–S44
Zsom A, Ormel CW, Güttler C et al (2010) The outcome of protoplanetary dust growth: pebbles, boulders, or planetesimals? II Introducing the bouncing barrier. A&A A57(22)